Sedimentology, stratigraphy and reservoir architecture of the Lower Triassic Main Buntsandstein in the Roer Valley Graben, the Netherlands

Cecchetti, E.; Martinius, A.W.; Felder, M.; Donselaar, M.E.; Abels, H.A.

DOI
10.1016/j.marpetgeo.2025.107519

Publication date
2025

Document Version
Final published version

Published in
Marine and Petroleum Geology

Citation (APA)
Cecchetti, E., Martinius, A. W., Felder, M., Donselaar, M. E., & Abels, H. A. (2025). Sedimentology, stratigraphy and reservoir architecture of the Lower Triassic Main Buntsandstein in the Roer Valley Graben, the Netherlands. *Marine and Petroleum Geology*, *182*, Article 107519. https://doi.org/10.1016/j.marpetgeo.2025.107519

Marine and Petroleum Geology 182 (2025) 107519

Contents lists available at ScienceDirect

Marine and Petroleum Geology

journal homepage: www.elsevier.com/locate/marpetgeo

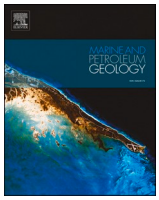

Sedimentology, stratigraphy and reservoir architecture of the Lower Triassic Main Buntsandstein in the Roer Valley Graben, the Netherlands

E. Cecchetti [a,*], A.W. Martinius [a,b], M. Felder [c], M.E. Donselaar [a], H.A. Abels [a]

[a] Department of Geoscience and Engineering, Delft University of Technology, Stevinweg 1, 2628, CN Delft, the Netherlands
[b] Equinor ASA, Arkitekt Ebbells 10, N-7053, Trondheim, Norway
[c] Molenaar GeoConsulting, Richard Wagnerlaan 11, 2253CA, Voorschoten, the Netherlands

ARTICLE INFO

Keywords:
Main Buntsandstein Subgroup
Sedimentology and stratigraphy
Reservoir architecture
Heterogeneities

ABSTRACT

The Main Buntsandstein Subgroup in the Roer Valley Graben in the southern Dutch subsurface is a sand-prone sedimentary interval deposited in a fluvial-aeolian environment, and is currently investigated for its suitability as target for low-entalpy geothermal exploration. The current depositional models in the Roer Valley Graben do not fully address the facies heterogeneities within and between Buntsandstein sedimentary units and their impact on the prediction of reservoir architecture. A detailed analysis of the Main Buntsandstein sedimentary facies heterogeneities to de-risk future sustainable energy operations is therefore crucial. In the present study, the sedimentology and lithostratigraphy of the Buntsandstein are assessed in a multidisciplinary analysis by use of a subsurface dataset composed of well cores, gamma-ray logs, and thin section data.

The deposition of the Main Buntsandstein sediments in the Roer Valley Graben is dominated by different fluvial processes, with minor aeolian reworking. River planform style evolved through geological time from highly mobile and ephemeral to more perennial in nature. These changes in river style seem to be dictated by a decrease in climatic aridity along with a decrease in tectonic activity.

The depositional processes resulted in the development of six lithofacies associations, developing three different types of reservoir architectures with their own set of heterogeneities at different spatial scales. Amalgamated, stacked sandstones have the highest net-to-gross (N/G) with a high degree of lateral and vertical connectivity, and the highest average porosity and permeability. Compensational-stacked sandstone reservoirs have a lower N/G and are the most heterogeneous due to the frequent occurrence of cemented intervals as well as mud drapes in the sandstone bodies. Marginal isolated sandstones show a well preserved relationship between reservoir properties and depositional facies, while more data are needed to resolve the spatial connectivity and lateral continuity of these sandstone bodies.

The results of this study enhance the understanding of Lower Triassic reservoir architecture and sedimentary heterogeneities in the Roer Valley Graben that can be applied well beyond the area and provide a solid basis for future investigation of the relationship between sedimentary facies, diagenesis, and reservoir quality.

1. Introduction

The Lower Triassic Main Buntsandstein Subgroup stands as a well-established clastic hydrocarbon reservoir and aquifer unit in the North Sea Basin and beyond. In the Netherlands, valuable hydrocarbon accumulations occur in the fluvial-aeolian sandstone reservoirs of the Main Buntsandstein Subgroup onshore and offshore (Bachmann et al., 2010). Sandstones from the Main Buntsandstein Subgroup have also attracted attention for their potential application in geothermal energy, leveraging their widespread distribution and favorable in-situ temperatures (Kramers et al., 2012; Hjuler et al., 2019; Mijnlieff, 2020). In the Roer Valley Graben in the southeastern Netherlands, sandstones with a total thickness up to ~200–250 m (Cecchetti et al., 2024), and in-situ temperatures up to 120–130 °C at depths of 2–3 km could provide energy for different applications such as district and greenhouse heating, and direct electricity use (Kramers et al., 2012; www.ThermoGIS.nl).

Several models provide insight into the depositional processes and resulting sedimentary structures in the Early to Middle Triassic in the Roer Valley Graben (Carter et al., 1990;Van Adrichem Boogaert and Kouwe, 1993 ; Geluk and Röhling, 1997; Geluk, 2005; Palermo et al.,

* Corresponding author. Department of Geoscience and Engineering, Delft University of Technology, Stevinweg 1, 2628, CN Delft, the Netherlands
E-mail address: emilio.cecchetti@sproule-erce.com (E. Cecchetti).

https://doi.org/10.1016/j.marpetgeo.2025.107519
Received 21 February 2024; Received in revised form 31 March 2025; Accepted 18 June 2025
Available online 20 June 2025

2008; IF Technology, 2012). However, most of the depositional models available for the Main Buntsandstein seem to be incomplete and somehow in contradiction with each other. For example, Carter et al. (1990) suggest deposition via fluvial fan systems with a northeast average paleoflow direction originating from a terrain source, the London-Brabant Massif, located to the southwest. Geluk (2005) proposes a model with deposition via axial river systems flowing to the northwest originated from the Armorican Massif. More recently, a model by IF Technology (2012) suggests that the Main Buntsandstein Subgroup was deposited as result of an interplay between fluvial fan systems sourcing from the London-Brabant Massif in the southwest and a terrain located on the northeast side of thethe Roer Valley Graben margin, and an axial river system with an average northwest paleoflow direction. The presence of different depositional models creates uncertainties as each model results in different sedimentary architectures with distinct geometries and spatial distribution of the sandstone bodies.

The origin and arrangement of these bodies introduce sedimentary heterogeneities at various scales from cm to km that can influence primary porosity, permeability, and subsequent secondary processes such as diagenesis (Hartmann et al., 1999; Morad et al., 2010; Ringrose et al., 2008). Busch et al. (2022) have documented the positive relationship between grain size and porosity and permeability in the Buntsandstein of the Upper Rhine Graben. More specifically, the variation in grain size and sorting between the foreset and bottomset within channel bar elements can result in fluid-flow anisotropy (Hartkamp-Bakker and Donselaar, 1993; McKinley et al., 2011). Furthermore, the presence of chemically reactive intraclasts, such as detrital dolomite clasts, can lead to early cement precipitation creating flow baffles (Molenaar and Felder, 2019; Bertier et al., 2022; Busch et al., 2022). These examples of heterogeneities can create flow anisotropies at different levels; thus, it is crucial to evaluate the presence of such heterogeneities and integrate them into reservoir architecture models (Ringrose et al., 2008; Larue and Hovadik, 2006).

The present study of the Main Buntsandstein Subgroup focuses on its development in the Roer Valley Graben (Fig. 1a). We perform a comprehensive sedimentological, petrographical and petrophysical analysis to understand the depositional origin, reservoir architecture, and sedimentary heterogeneities of the Main Buntsandstein Subgroup. This was possible by leveraging a publicly available data set (www.nlog.nl), along with a 20-m-long previously undescribed core from the southeastern region, and newly acquired thin section data from multiple wells. We conducted a sedimentological analysis of all well cores available to analyze the sedimentary facies and provide a better understanding of their genesis and distribution. These results integrated with petrophysical data allowed to study the architecture, heterogeneities, and quality of the potential reservoir units. This study contributes to the understanding of the Main Buntsandstein Subgroup reservoir architecture and heterogeneities in the Roer Valley Graben, and more in general it contributes to the understanding of Lower Triassic systems in northwestern Europe basins.

2. Geological setting

2.1. Tectonics and paleogeography

The Roer Valley Graben is 30–40 km wide and about 130 km long (Fig. 1a) and is bounded by a NW-SE oriented fault system that developed in the Carboniferous and was subsequently reactivated during later Mesozoic and Cenozoic tectonic events (NITG, 2004; Kombrink et al., 2012; Cecchetti et al., 2024). The Roer Valley Graben was an active depocenter for the Main Buntsandstein Subgroup. The accommodation space was created as a result of a series of short-lived tectonic pulses intermitted with regional thermal subsidence resulting in a NW-SE oriented half-graben structure with normal faulting and local depocenter development across the Roer Valley Graben where thickness changes up to 100 m occur (Geluk, 2005; Cecchetti et al., 2024). Tectonic activity decreases throughout the deposition of the Buntsandstein. Eventually, the Roer Valley Graben became a tectonically stable region where only a thin sequence (10–25 m) of Solling sediments were deposited (Geluk and Röhling, 1997).

During the Early to Middle Triassic, the Roer Valley Graben was located on the southwestern margin of the Germanic Basin (Fig. 1a), a

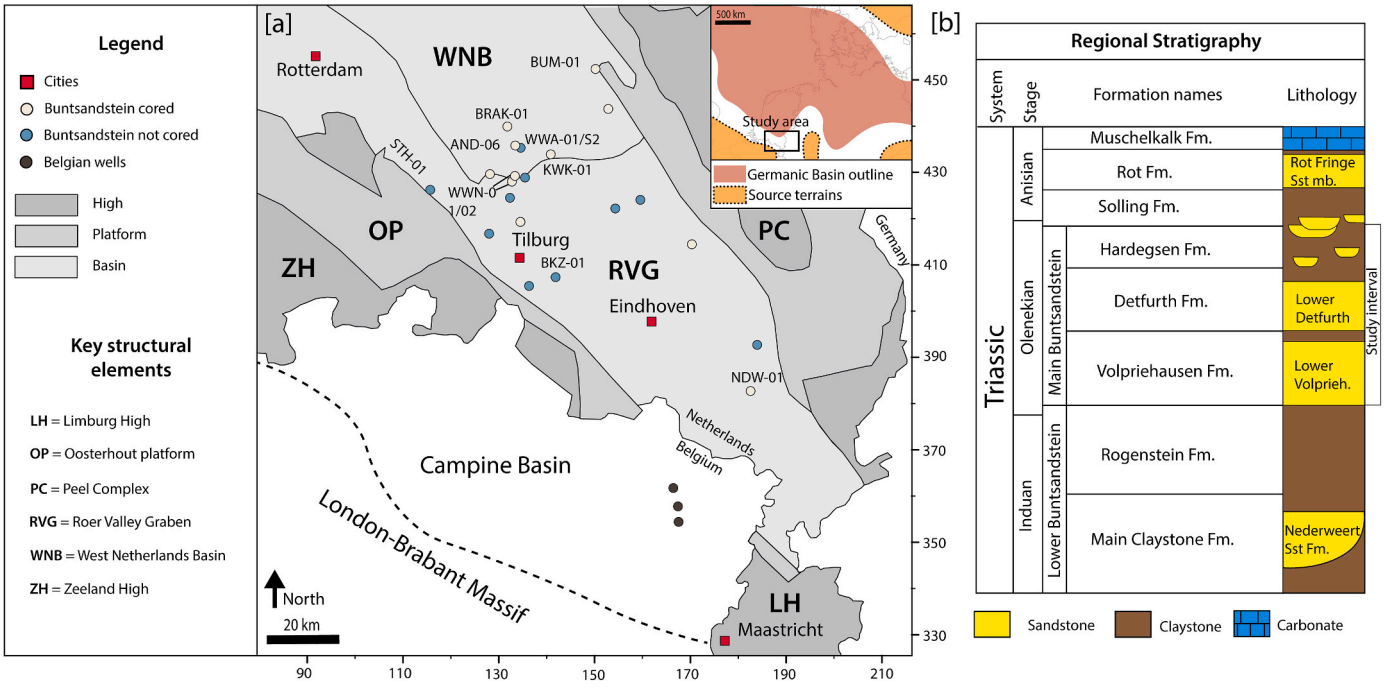

Fig. 1. a) The location of the study area with the main structural elements after Kombrink et al., 2012. Note that most of the cored wells are located in the northern part of the area, while in the southern part only one well (NDW-01) has part of the Buntsandstein stratigraphy cored. b) Triassic regional stratigraphy with over- and underburden after Van Adrichem Boogaert & Kouwe (1993).

large endorheic basin that developed during the Late Permian to Early Triassic and was located at the western margin of the Tethys domain (Scheck and Bayer, 1999; Ziegler et al., 2004; Geluk, 2005; Bourquin et al., 2011). The Germanic Basin was bounded by the Vindelician Highto the south and the Armorican and London-Brabant Massif to the west and northwest that fed sediments to the Roer Valley Graben (Ziegler, 1982; Geluk, 2005; Bourquin et al., 2011). To the north of the Roer Valley Graben, the Netherlands swell was a topographic high where little deposition occurred as confirmed by the thinner Buntsandstein sequence (~50 m) compared to the Roer Valley Graben (Geluk and Röhling, 1997; Bachmann et al., 2010).

The Main Buntsandstein Subgroup was deposited via river systems in the southwestern part of the Germanic Basin under arid climatic conditions as indicated by the widespread occurrence of aeolian facies and lack of diffuse paleosol development in many Triassic basins across Europe (Geluk, 2005; Bourquin et al., 2011). Water and sediments were supplied from the adjacent reliefs to the south, largely controlled by the amount of precipitation in the catchment areas as suggested by recent paleoclimatic simulations (Péron et al., 2005).

2.2. The Main Buntsandstein Subgroup

The sedimentation of the Main Buntsandstein Subgroup commenced at the Induan to Olenekian transition (Szurlies, 2004). In the Netherlands, the Main Buntsandstein Subgroup is part of the Lower Germanic Trias Group, and it is divided into three formations: Volpriehausen, Detfurth, and Hardegsen (Fig. 1b). The Volpriehausen and Detfurth Formations are usually formed by a lower fluvial/aeolian sandstone and an upper playa-lake silt/claystone (Van Adrichem Boogaert and Kouwe, 1993; Geluk and Röhling, 1997). The playa-lake silt/claystone units are thicker and better developed to the north (Kortekaas et al., 2018), while they can be absent close to the basin margin (Geluk, 2005).

The playa-lake sediments represent an important stratigraphic marker across the Netherlands and adjacent basins, generally considered to be deposited as a result of water table rise across the Germanic Basin (Geluk and Röhling, 1997; Bourquin et al., 2006). Such variation is interpreted to reflect sediment supply and water discharge fluctuation in response to climate changes upstream (Péron et al., 2005). The Hardegsen Formation is instead characterized by an alternation of sandstones and claystones at meter to tens of meter scale deposited through fluvial and lacustrine processes (Fig. 1b) (Van Adrichem Boogaert and Kouwe 1994) In the Netherlands, in general only the lower part of the Hardegsen Formation is preserved, while a complete succession has only be interpreted in the central part of the Germanic Basin (Geluk and Röhling, 1997).

The Main Buntsandstein Subgroup is ~200–250 m thick in the Roer Valley Graben and it is considerably thinner (~150 m) or locally absent due to erosion on the adjacent platforms/highs (Cecchetti et al., 2024). It overlies the Rogenstein Formation, a ~100 m succession of claystone and oolitic beds deposited in a near-shore, shallow water environment (Fig. 1b) (Palermo et al., 2000). The boundary between the Rogenstein and the Main Buntsandstein Subgroup is taken at the base of the first sandstone bed (Van Adrichem Boogaert and Kouwe, 1993).

Above the Main Buntsandstein Subgroup, the Solling Formation consists of sandstone and claystone units deposited in a fluvial-lacustrine environment (Geluk, 2005). In the Netherlands, the Solling Formation is the lowermost unit of the Upper Germanic Trias Group (Van Adrichem Boogaert and Kouwe, 1993). The boundary between the Hardegsen and Solling Formations is easily discernible when associated with the Hardegsen Unconformity, an angular unconformity induced by tectonics that is responsible for the erosion of Lower Triassic sediments in part of the Germanic Basin (Geluk, 2005). However, in the Roer Valley Graben, the Hardegsen Unconformity is not observed, and the sandstones of the Solling Formation are stacked conformably on top of the sandstones of the Hardegsen, making the boundary between the Hardegsen and Solling Formations difficult to discern (Fig. 1b).

3. Material and methods

The present study is based on the analysis of core, rock samples and petrophysical data from 24 wells in the Roer Valley Graben (Fig. 1a). Lithofacies, sedimentary structures, sediment composition, and texture were evaluated from slabbed cores, cuttings, and thin sections. A well-log correlation was conducted across the study area to determine the Buntsandstein lithostratigraphy in the area and assess reservoir architecture. Porosity and permeability data from publicly available dataset (www.nlog.nl) were integrated to assess the reservoir quality of the different lithofacies types, and to assess the characteristics and scale of heterogeneities such as permeability baffles, and barriers.

3.1. Core and cutting analysis

A total of 382 m of core material from the Main Buntsandstein Subgroup was described from 9 wells across the Roer Valley Graben (Fig. 1a and Table 1). In the Waalwijk-North (WWN-01-S2) well, ~72 % of the Main Buntsandstein Subgroup stratigraphy is covered by core material, providing a relatively continuous record to analyze the changes in sedimentary structures and heterogeneities through the stratigraphy (Table 1). The well inclination, ranging between 0 and 35°, was taken into account to establish the true stratigraphic thickness (TST) of the lithofacies types. Grain size for the core samples was determined with a grain-size chart under a hand lens.

The analyzed sediments were subdivided in lithofacies types defined by macroscopic characteristics. The lithofacies types were clustered into lithofacies associations representing assemblages of spatially and genetically related lithofacies deposited in a particular sub-environment. For the wells where core samples were not available, rotary and PDC (Polycrystalline Diamond Compact) cuttings were used in combination with mud logs to determine sediment characteristics such as colour, grain size, and composition.

Preserved dune-scale cross-set thickness (Sm) was used to estimate the mean bedform height (*Hm*) through the following empirical equation following Bridge and Tye (2000) and Leclair and Bridge (2001):

$$Hm = 2.9^{*}(\mp 0.7)^{*}Sm \quad (1)$$

The resulting bedform height (*Hm*) measurements were used to estimate the formative bankfull depth (Bd) using Eq. (2) after Bradley and Venditti(2017):

$$Bd = 6.7^{*}Hm \quad (2)$$

Due to the absence of borehole images, the foreset laminae dip angle was interpreted relative to truncation surfaces and to sedimentary structures estimated to be deposited horizontally (e.g. claystone lamination). The bankfull depth was then used to calculate channel belt width (*CBW*) for braided fluvial systems following Fielding and Crane (1987) through the following equation:

$$CBW = 513^{*}B \quad (3)$$

3.2. Thin section study

Sediment texture and composition of 63 thin sections from 6 wells were studied with an optical microscope. In addition, petrographic legacy data of 32 thin sections from 3 wells available via www.nlog.nl were integrated into the study (Table 1). The thin sections were representative of most of the studied core material, giving the average sampling rate ranging from 0.5 to 6.5 m. The diameters of 100 grains per sample were measured to determine grain-size distribution and sorting following Folk and Ward (1957). Sediment composition was studied through the Gazzi-Dickinson point-counting method (200 points per thin section). Point-count results were grouped following Pettijohn

Table: 1
Summary of the rock samples data available to the study. Note that only well WWN-01-S2 has an appropriate core recovery that allowed to study vertical changes in sedimentary facies throughout the Buntsandstein stratigraphy. Thin sections from different studies have been integrated with the data produced within this work. Different authors are represented by the following symbols: * GAPS well reports; **This study; *** Carter et al. (1990). The works by GAPS and Carter et al. (1990) can be downloaded from www.nlog.nl.

Well name	Top Buntsandstein (MD)	Bottom Buntsandstein (MD)	Top Cored interval (MD)	Bottom Cored interval (MD)	Cored interval (MD)	Core recovery	Thin Sections studied	Author	Plugs measured
Andel-06 (AND-06)	*2867.12*	*3136*	*2894*	*2910.65*	*16.65*	*6.19 %*	*4**	*GAPS*	*33*
Brakel-01 (BRAK-01)	*2446*	*2637*	*2452*	*2477*	*25*	*13.09 %*	*6**	*GAPS*	*85*
Buurmalsen-01 (BUM-01)	*1368.74*	*1576*	*1498*	*1531*	*33*	*15.92 %*	*29***	*This study*	*91*
Keerwijk-01 (KWK-01)	*2547*	*2754*	*2548*	*2601.63*	*53.63*	*25.91 %*	*20***	*This study*	*160*
Keldonk-01 (KDK-01)	*2076*	*2287.93*	*2258*	*2275.1*	*17.1*	*8.07 %*	*4**	*GAPS*	*79*
Nederweert-01 (NDW-01)	*2030*	*2237.12*	*2120.5*	*2135*	*14.5*	*7.00 %*	*12***	*This study*	*23*
Sprang Capelle-01 (SPC-01)	*2607.62*	*2756.5*	*2647*	*2675*	*28*	*18.81 %*	*9***	*This study*	*80*
Varik-01 (VRK-01)	*1623*	*1810.57*	*1656.5*	*1660.73*	*4.23*	*2.26 %*	*7***	*This study*	*12*
Waalwijk North-01-S2 (WWN-01-S2)	*3166.23*	*3355*	*3169*	*3305.5*	*136.5*	*72.31 %*	*22****	Carter et al. (1990) *(BP)*	*536*

(1975) and plotted in a ternary diagram (QFL).

3.3. Well log correlation

The gamma-ray log was used to explore the Main Buntsandstein lithostratigraphy between wells. The aims were to assess the spatial variation of the different lithofacies associations and to explore the 2D potential reservoir architecture. In the absence of chronostratigraphic markers (e.g. biozones) lateral correlation at the scale of the study area is highly uncertain. For this reason, a lithostratigraphic correlation of the individual sandstone bodies was only attempted between wells at distances shorter than 1.5 km.

First, in the cored wells, a core-to-log shift was applied to correct for potential depth misfit between the sedimentological log created from the core study and the gamma-ray log. Secondly, a characteristic GR log profile was determined for each lithofacies association in the cored wells. Subsequently, these GR log patterns were extrapolated to non-cored wells and depth intervals were assigned to particular lithofacies associations. This was done with the help of cuttings where available. Thereafter, variations in the thickness of the lithofacies associations between wells were identified and a lithostratigraphic framework was tentatively established.

4. Results

4.1. Sedimentology of the Buntsandstein in the Roer Valley Graben

Twelve lithofacies types were identified based on grain-size distribution, lithology, texture, and sedimentary structures in full cores and core slabs (Fig. 2 and Table 2). There are two gravel lithofacies named: homogenous to crudely-stratified gravel (G) and stratified gravel (Gs); six sandy lithofacies: pebbly sandstone (Slx), cross-stratified sandstones (Sx), horizontally-stratified sandstones (Sh), ripple cross-laminated sandstone (Sl), bioturbated ripple cross-laminated sandstones (Slb) and homogeneous sandstones (Sm); and four silty/muddy lithofacies: laminated to homogeneous claystone (F), bioturbated claystone (Fb), bioturbated heterolithic mud, silt, to sand (Fib), pedogenetic claystone/siltstone (Fp). The twelve lithofacies were grouped into six lithofacies associations based on vertical successions and geometrical arrangement; four gravelly to sandy lithofacies associations (LA-1 to LA-4) and two muddy lithofacies associations (LA-5 and LA-6).

4.1.1. Stacked stratified sandstone (LA-1)

Lithofacies association 1 (LA-1) is composed of very-fine to coarse-grained sandstones with conglomerate (G and Gs) occasionally found at the base (Fig. 3a and b). Sandstones are usually greyish (GLEY 1 8/N). However, in the eastern part of the basin, these can be orange to red (5 YR 6/4), oxidized with presence of hematite coating (Fig. 3a). LA-1 is usually multistoried forming stacked complexes over of tens of meters in thickness, where each storey has an average thickness of 3.7 m and a standard deviation of 1.4 (Fig. 9b). Within each storey, coarse to medium-grained pebbly sandstones (Slx) can be found at the base, bearing intrabasinal fragments, such as mud chips, silt-sandstone grains, and dolomite grains (Fig. 3a and d). Mud chips are usually angular and elongated, reaching 2–3 cm in diameter. Silt-sandstone and dolomite grains are subrounded, which diameter can reach up to 1–2 cm in length. Unfrequently, pebbly sandstone (Slx) can be found superimposing thin (<0.5 m) gravel lithofacies (G and/or Gs) developing a sharp contact with the underlying sediments. The bulk of each storey is composed of moderately-to well-sorted cross-stratified sandstones (Sx) and horizontally-stratified sandstones (Sh) together accounting for ~ 75 % of the total lithofacies assemblage in LA-1 (Fig. 9a). Cross-stratified sets (Sx) can reach thickness of ~45 cm and can be organized in cosets reaching thicknesses up to 5 m. Within each set, foresets can bear elongated mud chips of few cm in size at the base. Bottomsets can reach thickness of 3–4 cm and they are usually formed by very fine to fine-grained sandstones. Bottomset sandstones can be horizontally-laminated or cross-laminated with ripple structures (Fig. 3c).

Cross- and horizontally-stratified sandstone (Sx and Sh) can be characterized by a bimodal grain-size distribution organized in pairs of laminae with a thickness of 0.2–1 cm (Fig. 4a and c). When this occurs, usually grains are coated with hematite. Each pair of laminae has a sharp flat base, while the boundary between the laminae is gradational. The lower laminae is usually moderately to well-sorted, rounded to well-rounded, medium to coarse-grained. The upper laminae consists of moderately sorted, subrounded to rounded, very fine to fine-grained sand.

At the top of each storey, ripple cross-laminated sandstones (Sl) are found, which may be overlain by very thin, usually thinner than 10 cm, beds of homogenous to laminated claystone (F). Ripple cross-laminated sandstones can show distinctive ripples (Fig. 3a). On the gamma-ray, LA-1 is characterized by a rather blocky shape, with values that rarely exceed 90 API (Fig. 3e).

Petrographic analysis on 35 samples from LA-1 reveals that sandstones are mostly sublitharenites, with few samples that can be classified

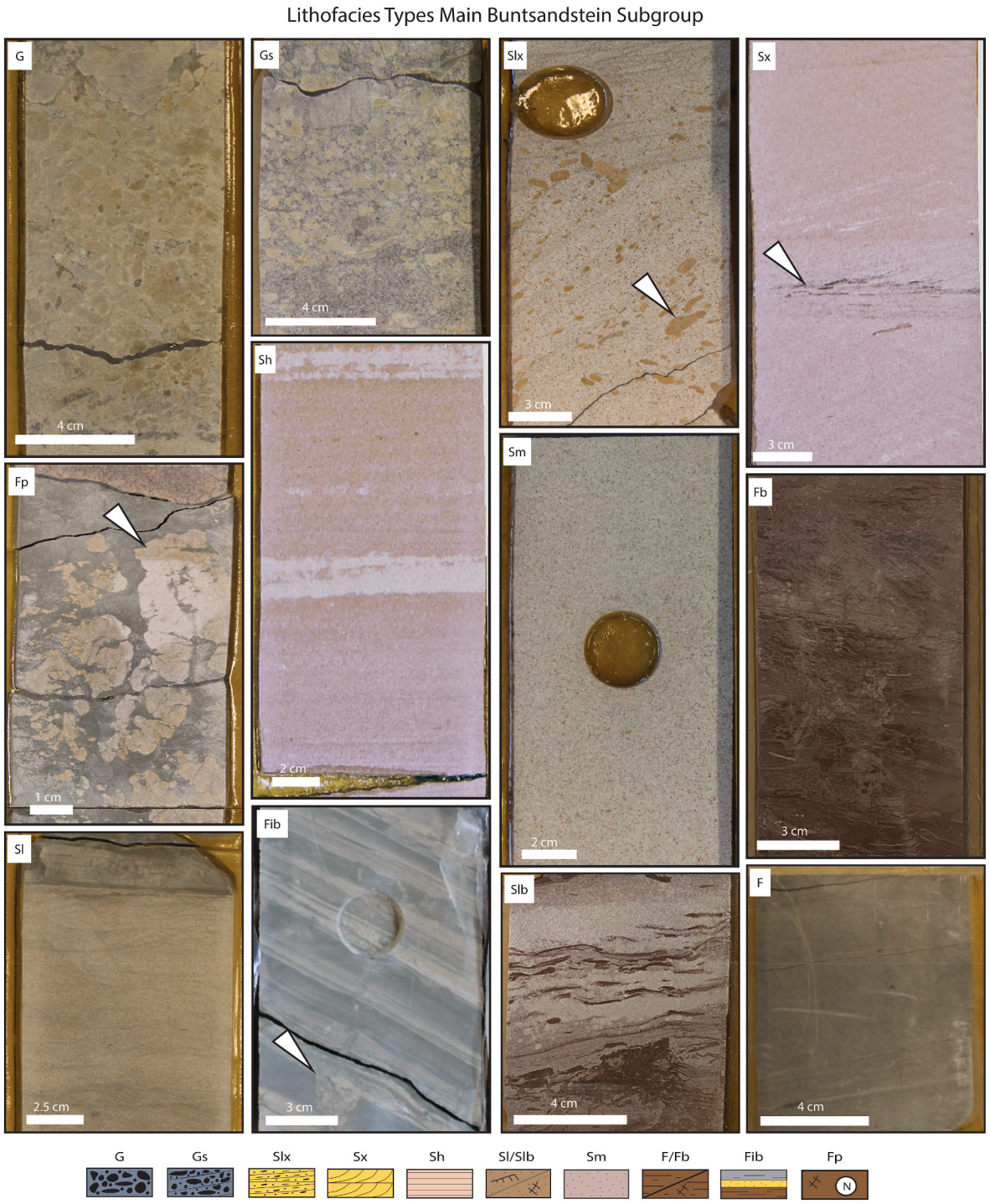

Fig. 2. Lithofacies types recognized in the study area. (G) Massive to crudely- stratified gravel. (Gs) Stratified gravel. (Slx) Pebbly sandstone. The arrow indicates a dolomite detrital grain. (Sx) Cross-stratified sandstone. The arrow indicates the set boundary with small mud chips aligned along the foreset direction. (Sh) Horizontally-stratified sandstone. (Sl) Ripple cross-laminated sandstone. (Slb) Bioturbated ripple cross-laminated sandstone. (Sm) Homogeneous sandstone. (F) Laminated to homogeneous claystone. (Fb) Bioturbated claystone. (Fib) Alternated bioturbated clay, silt, and sandstone. The arrow indicates a mud crack. (Fp) Pedogenic mud/siltstone. The arrow indicates pedogenic dolomite nodules.

as litharenites and subarkoses (Fig. 8b). Lithic fragments range from 5 to 50 % of the total detrital composition, where silt/sandstone and dolomite detrital grains represent the most dominant clasts.

134 measurements of preserved cross-set (Sx) thickness allow the reconstruction of bankfull flow depth of ~2.2 ± 1.283 m following Bridge and Tye (2000) and Bradley and Venditti (2017).

Interpretation: The abundance of cross-stratified sandstones in LA-1, the presence of intraclasts, and moderate sorting in a continental setting suggest deposition via fluvial processes. The different sedimentary structures encountered in LA-1 indicate these rivers had variable discharge velocities. Cross-stratified sets and co-sets (Sx and Sxl) compose channel floor elements suggesting deposition under a lower flow regime. Horizontal-stratified (Sh) and ripple cross laminated sandstones (Sl and Slb) usually compose the top of subaqueous bedforms and indicate deposition under lower flow regime (Fielding, 2006). The fine-grained ripple cross-laminated (Sl) sandstones on top of

Table: 2
Description and interpretation of the lithofacies types in the Main Buntsandstein Subgroup.

Lithofacies name	Description	Statistics	Interpretation
Massive to crudely stratified gravel (G)	Pebble- to cobble-size gravel with an undefined structure to crude horizontal stratification. This lithofacies is composed by granules- to cobble-size intraclasts that are moderately to poorly sorted. The intraclast lithology ranges from mudstone, silt/sandstone, and dolomite. Locally, a bimodal texture may occur with fine to medium-grained angular to sub-rounded sandstone as matrix. Rarely, clay, silt, or cross-stratified sandstone lenses may be interbedded with gravels.	**Unit thickness** mean = 0.13 m std = 0.1 m	Reworking of intrabasinal clasts of floodplain mudstones, silt/sandstones, or dolomite, transported and redeposited quickly by high-energy, turbulent unidirectional flows. The unsorting, massive- to crudely-stratified character may indicate channel-lag deposition through debris flow (Miall, 1977). The frequent superimposition of stratified gravel (Gs) suggests sediment organization into bedforms (Nichols, 2009).
Stratified gravel (Gs)	Stratified gravel makes up beds of granules- to cobble-size intraclasts. The intraclast lithology ranges from mudstone, silt/sandstone to dolomite. Bimodal texture may occur with fine to medium-grained angular to sub-rounded sandstone as matrix. This facies is usually organized in normally-graded cross-stratified sets, where clasts lay on the foreset slopes. Reactivation surfaces may be present. Individual sets are usually separated by inclined surfaces with an angle larger than 5°. Usually, the sorting within each set increases upwards. Planar to trough strata cannot be distinguished due to the bidimensionality of the core samples and poor spatial resolution. Dolomite cement may be pervasive and alter the primary sedimentary structure.	**Set thickness** mean = 0.12 m std = 0.07 m **Coeset thickness** mean = 0.26 m std = 0.25 m	Eroded mud and carbonate clasts transported and redeposited by high energy, turbulent unidirectional flows during plane bed migration, associated with channel lags. The presence of cross-stratification indicates the individual strata were produced by avalanching movements of clasts on downward or lateral flanks (Miall, 1981; Yagishita, 1997; Steel and Thompson, 1983).
Pebbly sandstone (Slx)	Fine- to coarse-grained, commonly bearing granule-size intraclasts, cross-stratified sandstones. The intraclast lithology varies from mudstone, silt/sandstone to dolomite. This facies can be either found as a solitary set or organized coesets. Contact between foresets laminae and lower bounding surface is usually tangential. Periodic, thick, coarse cross-strata may occur within singular sets. Overall, the foresets differ in grain size and are locally cut by reactivation surface. Convex set boundaries can occur. This facies overlies scour surfaces at the base of channels and may occur at the base of macroforms within channel sandstones.	**Set thickness** mean = 0.15 m std = 0.05 m **Coeset thickness** mean = 0.63 m std = 0.45 m	Migration of (3D) sinuous subaqueous dunes under upper to lower flow regime. The presence of intraclasts and unsorted basal deposits suggests erosion and transportation of antecedent deposits and incorporation into bottomset architecture (Herbert et al., 2018).
Cross-stratified sandstone (Sx)	Fine to medium-grained, well-rounded, and moderate- to well-sorted planar cross-stratified sandstone. Locally, bimodal grain-size distribution is observed. Set boundaries are flat and sharp. Usually, set thickness decreases upward. However, it depends on the preservation potential. Foresets represent avalanching slopes. Occasionally showing bimodal grain size distribution in the foresets, with coarser foresets that may have been cemented by later diagenesis. Finer laminae in the foresets can be micaceous. Bottomsets can show horizontal laminations or ripples. Contact between foresets laminae and lower bounding surface is usually abrupt.	**Set thickness** mean = 0.11 m std = 0.06 m **Coeset thickness** mean = 0.94 m std = 0.89 m	Subaqueous (2D) dune migration under lower-flow regime unidirectional flows, associated with the channelized flow. The evidence of flow brief pauses in sand transport (mud drapes) indicate periodic emersion/very shallow water level (Herbert et al., 2018). In NDW-01, these dunes can be subaerial and shaped by the action of wind with suspension and saltation lamina pairs (Fig. 4) (Henares et al., 2014).
Horizontally-stratified sandstone (Sh)	Very fine- to coarse-grained sandstone, well-rounded, moderately to well-sorted, occasionally bearing pebble-granule size clasts. The units of this lithofacies are represented by isolated sets or coesets of parallel to low-angle cross strata that range in thickness from 0.045 to 1.7 m. The distinction between horizontal and low-angle cross-stratified could not, or only seldom, always be done due to well path deviation and small spatial resolution of the core samples. Strata sets may be separated by slightly inclined (<5°) truncation surfaces in coesets.	**Set thickness** mean = 0.12 m std = 0.04 m **Coeset thickness** mean = 0.47 m std = 0.36 m	This facies is formed by a transition from lower to upper flow regime. Horizontal stratification forms at low flow velocity for medium to coarse grain sizes, with dune bedforms start developing as flow speed increases (Nichols, 2009).
Ripple cross-laminated sandstone (Sh)	Very fine- to medium-grained sandstone, with the rare occurrence of medium- to coarse-sand. The base is often gradational. The top is sharp or erosive. Asymmetrical to symmetrical wave ripple lamination commonly develop, including mud-draped bidirectional bedforms. Flaser to wavy beddings may occur, bounded by mud and silt. This facies can be organized in solitary sets or coesets of ripple-scale cross laminae.	**Unit thickness** mean = 0.17 m std = 0.15 m	Sediment transport occurs under a lower flow regime(Miall, 1977; Nichols, 2009). Deposition may have occurred within fluvial channels or pond/lake, with water oscillation induced by wind.
Bioturbated ripple cross-laminated sandstone (Slb)	Very fine to fine cross-laminated sandstone. Burrows (Palaeophycus and maybe Planolites), mud cracks and rootlets that may obscure primary sedimentary structures. Asymmetrical to symmetrical wave ripple lamination frequently occurs, with mud drapes and clay chips. This facies forms units with an average thickness of 31 cm, however, they can stack up to a meter.	**Unit thickness** mean = 0.31 m std = 0.26 m	Sediment transport occurs under a lower flow regime (Miall, 1977; Nichols, 2009). Deposition may have occurred within fluvial channels or pond/lake, with water oscillation induced by wind. The presence of desiccation and bioturbation suggests periodical emersion and an environment favorable for subaqueous life (Buatois et al., 1998).
Homogeneous sandstone (Sm)	Fine to medium grain size sandstone, moderately to well sorted. It may bear pebbles size clasts. Usually, top and bottom boundaries are sharp or erosive. Sandstone is mostly structureless, however, orientated pebble size clasts and faint lamination are visible. Burrows rarely occur.	**Unit thickness** mean = 0.34 m std = 0.2 m	High rate of deposition during high discharge periods or sediment reworking from biological activities.

(*continued on next page*)

Table: 2 (*continued*)

Lithofacies name	Description	Statistics	Interpretation
Bioturbated heterolithic mud, silt to sand (Fib)	This facies is formed by mm to cm (<5 cm) alternation of mudstone/siltstone with fine to coarser sandstone. Beds can be lenticular to wavy. Sandstone can be homogenous to laminated. Current ripples can occur together with abundant mud drapes. Mud cracks, rootlets, and burrows (Palaeophycus and maybe Planolites) are frequent that may overprint primary sedimentary structures. The color of the mud changes from brownish (7.5 YR 2.5/3) to red (10R 4/8) and/or greyish (GLEY 1 6/5G). Desiccation cracks can reach lengths up to 5 cm. This facies is organized in units reaching up to meter scale, with a mean of around 25 cm.	**Unit thickness** mean = 0.27 m std = 0.24 m	Low flow regime, deposition from suspension alternated with periodical inputs of sand transported by current. The environment of deposition was favorable for subaqueous life, periodically drying up (Buatois et al., 1998). Deposits of waning floods, overbank deposits, lakes, or ponds (Miall, 1977; Mckie, 2011; Coronel et al., 2020).
Laminated to homogeneous claystone/siltstone (F)	Clay to siltstone with laminated to homogeneous structure. The lithofacies is reddish (2.5 YR 4/2), brownish (7.5 YR 2.5/3) and/or greenish (GLEY 2 6/10G), occurring in isolated units ranging from 2 to 40 cm in thickness. The top boundary is generally erosional. The bottom can either is often sharp, but can also be gradational.	**Unit thickness** mean = 0.11 m std = 0.11 m	Deposition from suspension during waning flows within a channel, or in a floodplain under a temporary water level (Miall, 1977).
Pedogenic mudstone/ siltstone (Fp)	Mudstone to siltstone with laminated to homogeneous structure. Structureless to faint laminated very fine sand intervals can also be interbedded. The lithofacies is reddish (5 YR 4/4) or greyish (GLEY 1 5/N). It usually exhibits a mottled aspect and paleosol development. The frequent presence of dolomite nodules and bioturbation often overprint primary structures. Top boundaries are erosional, while the bases are often gradational. This facies is organized in isolated units reaching up to 1.2 m in thickness.	**Unit thickness** mean = 0.7 m std = 0.33 m	Deposition from suspension. Soil formation may occur with chemical precipitation developed on overbank fines. (Kraus, 1999; Pimentel et al., 1996).
Bioturbated claystone (Fb)	Bioturbated mudstone to siltstone. Primary structures are overprinted, however, locally this lithofacies can have laminated to homogeneous structures. Rootlets and burrows (Palaeophycus and maybe Planolites) are frequent. Mud cracks can occur. Structureless to faint laminated very fine sand can be interbedded. The color of lithofacies from brownish (7.5 YR 2.5/3) to red (10R 4/8) and/or greyish (GLEY 1 6/5G). It is organized in isolated units ranging from 5 to 70 cm in thickness, with a mean of 20 cm.	**Unit thickness** mean = 0.19 m std = 0.19 m	Deposition from suspension during waning flows within a channel, or in a floodplain under a temporary water level favorable for subaquatic life (Buatois et al., 1998). Periodically emersion led to mud crack formation.

cross-stratified sandstone (Sx) might represent bars that fine upwards into supra-platform deposits with periodical emergence (Steel and Thompson, 1983). Laminated claystone draping upper bar topography records deposition under very low energy discharge via suspension settling (Bridge, 2006).

In well NDW-01, to the southeast, the occurrence of oxidized sandstones with pairs of laminae that show normal grading and bimodal grain size distribution suggests subaerial exposure with aeolian sediment transport by saltation and suspension (Henares et al., 2020). This would indicate that fluvial sediments were periodically reworked and deposited through aeolian process, possibly in an interfluvial environment as recorded in many dryland settings (Mountney and Thompson, 2002; Bourquin et al., 2009; Cain and Mountney, 2009; Henares et al., 2014).

The dominance of medium to coarse-grained bedload material, the absence of fining-upward profile, the cm-to dm-scale thickness preservation of the cross-stratified sets, the near absence of preserved mudstone and the high degree of amalgamation indicate that LA1 was deposited by rivers that were shallow and highly mobile (Steel and Thompson, 1983; Gibling, 2006; Sambrook Smith et al., 2006; Bourquin et al., 2009; Limaye, 2020). This may be related to: i) a high energy braided fluvial system and the presence of non-cohesive erodible banks (North and Taylor, 1996); ii) high rate of deposition as result of ephemeral flows and low accommodation rate that forced the rivers to frequently shifting thereby eroding the floodplain (Mackey and Bridge, 1995; Bryant et al., 1995; Postma, 2014).

4.1.2. Fining-upward sandstone (LA-2)

Lithofacies association 2 (LA-2) is composed of very-fine to medium-grained sandstones organized in fining-upward successions with gravel lithofacies (G and Gs) observed at the base (Fig. 5a and b). LA-2 occurs either as single units of 2–3 m in thickness (Fig. 9b) vertically enclosed between floodplain deposits or stacked on top of each other composing multi-storey intervals of up to 6–7 m thickness. The lower part of each storey is formed by sharp-based gravel lithofacies (G and/or Gs) or pebbly cross-stratified medium to fine-grained sandstones (Slx). These lithofacies types usually contain poorly sorted, subangular to subrounded mud chips, silt/sandstone and dolomite clasts with diameters that can reach up to 3–4 cm (Fig. 5c and d). Locally, large (4–5 cm) mud clasts are present within the gravel lithofacies. The central part of the lithofacies association is characterized by an internal arrangement of stacked sets of medium to very fine-grained, moderately to well-sorted cross-stratified sandstones (Sx). The cross-bed sets can form cosets reaching ~2 m in thickness. These sandstones may occasionally bear dolomite clasts, micas and mud chips (Fig. 5a). These are usually subrounded to subangular and below cm-scale, oriented with their longest axis parallel to the foresets. Foresets are either angular or tangential at their bases, lying over bottomsets that can be horizontally or cross-laminated with ripple structures. Cross-stratified sandstones (Sx) may be interbedded at dm to m scale with horizontally-stratified sandstones (Sh) and structureless sandstones (Sm). The upper part of this lithofacies association is dominated by fine-grained ripple cross-laminated sandstones (Sl) grading up into muddy lithofacies. This fine-grained upper section can be bioturbated by insect burrows and rootlets. Locally, claystone can be found directly superimposing the lower part of this lithofacies association. On the gamma-ray, LA-2 typically has a bell shape bounded by high gamma-ray readings at the top (Fig. 5e).

Thin section analysis reveals that samples are mostly litharenites to sublitharenites (Fig. 8b). Rock fragments can make up to 40–50 % of the total detrital components, with dolomite and silt/mudstone clasts representing the most abundant classes. An average dune-scale bedform thickness of ~0.6 (±0.7) m based on 58 set thickness measurements

suggests a bankfull depth in the order of ~4.3 m ± 3.692 m (cf. Bridge and Tye, 2000; Bradley and Venditti, 2017).

Interpretation: The vertical assemblage of lithofacies suggests that these sediments have been deposited by fluvial processes. This lithofacies association is dominated by lithofacies (G, Gs, Slx and Sx) deposited mostly via bedload transport under medium to high-flow discharge (Bridge, 2006). The muddy upper sections of the fining-upward cycles were periodically exposed and locally vegetated, as shown by the presence of rootlets and vertical burrows produced by insects. The fining-upward trends of grain sizes, reconstructed bankfull depth of average ~3–4m based on bedform height measurements, presence of bioturbation and preservation of overbank deposits with paleosols suggest a rather perennial nature of these rivers potentially induced by the higher stability of the banks and a less ephemeral discharge.

The presence of poorly-sorted gravel lithofacies (G and Gs) with intraclasts at the base of the sandstone bodies indicates the fill of erosional scours in response to channel incision into adjacent floodplain areas (Gómez-Gras and Alonso-Zarza, 2003). The abundance of argillaceous and dolomite clasts suggests erosion of muddy-dominated floodplains with indurated dolocrete nodules. Locally, the superposition of overbank facies over gravel (G and Gs) and cross-stratified sandstones (Slx and Sx) indicates channel migration or abrupt loss of stream power and infilling of abandoned channels (Toonen et al., 2012).

4.1.3. Coarsening-up sandstone (LA-3)

Lithofacies association 3 (LA-3) consists of very-fine to fine-grained, moderately to well-sorted sandstones organized into coarsening-upward successions (Fig. 6a and b). This lithofacies association occurs only in the BUM-01 well in the northern section of the study area (Fig. 1a). The lower part of LA-3 is characterized by an alternation of fine to very-fine ripple cross-laminated sandstones (Sl and Slb), intercalated at cm to dm scale within horizontally-stratified sandstones (Sh), structureless sandstones (Sm), and bioturbated heterolithic deposits (Fib). The heterolithic sediments bear mud cracks and show evidence of soft sediment deformation (Fig. 6a). The upper part of this lithofacies association is characterized by an alternation at m scale of fine to very-fine, cross-stratified sandstones (Sx) and horizontally-stratified sandstones (Sh), which respectively account for 52 and 25 % of LA-3 (Fig. 9a). These stratified sandstones are usually fine to medium grained and can present a bimodal grain-size distribution organized in pairs of laminae, where the coarser laminae are usually better sorted than the finer ones. The cross-stratified sandstone individual sets are on average 10 cm thick, while the entire sandstone unit can reach up to 3–4 m in thickness (Fig. 9b). LA-3 is characterized by a funnel wireline profile, with values below 90 API generally found at the top where the cross-stratified sandstones (Sx) occur (Fig. 6f).

The analysis of 11 thin sections indicates that sandstones of LA-3 are litharenites (Fig. 8d) They are composed of mono- and polycrystalline quartz, and mudstone, dolomite, and silt/sandstone fragments usually smaller than 0.5 cm in diameter. Small anhydrite and/or gypsum nodules (<1 cm) are often present in the cross-stratified sandstones (Sx) of this lithofacies association (Fig. 4d). The detrital grains are mostly coated with hematite, which gives them a red/brown colour (Fig. 6 and c).

Interpretation: Ripple cross-laminated bioturbated sandstones (Slb) and horizontally-stratified sandstones (Sh) are interpreted to have formed from shallow, unconfined flow. The occurrence of Slb and Sh above muddy units (Fib and Fb mainly) indicates a low energy environment, with periodic input of sand transported by traction current. In this context, the mud cracks and hematite coatings suggest periodical subaerial exposure (Walker, 1979). The coarsening upward nature of LA-3 and the presence of heterolithic sediments above and below this facies association are interpreted to be the result of the progradation of the fluvial system into a floodplain area.

Considering the northern position in the basin, the widespread hematite coating, the fine grain size, and the relatively low thickness of the sandstone units, LA-3 is interpreted to be part of terminal-splay complex coalescing into a large arid plain. Similar deposits are as described in ancient and present-day analogues (Parkash et al., 1983; Nichols and Fisher, 2007; Fisher et al., 2008; Cain and Mountney, 2009; McKie, 2011; Voigt, 2017; Donselaar et al., 2022).

4.1.4. Thin-bedded sandstone (LA-4)

Lithofacies association 4 is characterized by thin-bedded (~0.6 m ± 0.5), very-fine to medium-grained sandstones (Figs. 7a and 9b). This lithofacies association is usually embedded in overbank facies (e.g. LA-6). It has a sharp lower boundary, while the upper boundary can be gradational into a sandstone from LA-1 or LA-2. The lower part of LA-4 is usually composed of pebbly (Slx) and structureless sandstones (Sm) (Fig. 7a). These lithofacies can contain angular to subrounded intraclasts that range in diameter from few mm up to 3 cm. The sediments where dolomite clasts are abundant are usually cemented (Fig. 7a). Cross-stratified and structureless sandstones are overlain by horizontally-stratified (Sh) and ripple cross-laminated (Sl and Slb) sandstones. LA-4 shows gamma-ray values around 100 API (Fig. 7c). The 4 thin sections studied for LA-4 reveal a detrital composition where quartz grains account on average for 76 %, silt/mudstone clasts for ~14 % and feldspars for ~8 % (Fig. 8d).

Interpretation: This lithofacies association is interpreted to be formed as a consequence of unconfined flow conditions on the floodplain associated with erosion of the channel levée (Fisher et al., 2007, 2008). In the Roer Valley Graben, this element is usually found in association with channel complexes, suggesting an origin as crevasse splay or terminal splay of the channel (Tooth, 2005). Their sharp basal contact is an indication of high flow energy, supported by the occurrence of rip-up mud clasts and dolocrete clasts in the lower part of LA-4 transported as bedload material.

4.1.5. Heterolithics (LA-5)

This lithofacies association is characterized by mm to cm scale alternations of bioturbated claystones and sandstones (Fib, Fb), (bioturbated) ripple cross-laminated sandstones (Slb) (Fig. 6a and b). Horizontally-stratified sandstones (Sh) and homogeneous sandstones (Sm) rarely occur. Lamination can be lenticular to wavy. Claystone can be reddish (5 YR 4/4), brownish (7.5 YR 2.5/3) to greyish (GLEY 1 6/5G) in colour (Fig. 6a–c and d). Injection structures and mud cracks are encountered (Fig. 6d) and are usually few cm in vertical length and diameter. These structures are infilled with sand or silt. Burrows and rootlets are occasionally encountered (Fig. 6a and c). Burrows are usually 3–4 cm in length, while rootlets can reach 10–15 cm. LA5 is characterized by an alternation of high (>125 API) and intermediate (100> API >125) readings (Fig. 6f). This lithofacies association can be up to 10 m thick when composed of multiple beds. Fib and Slb represent the most dominant lithofacies, accounting for 49 % and 28 % of the lithofacies assemblage (Fig. 9a).

Interpretation: The heterolithic sediments of LA-5 record episodic density currents formed in a low-energy environment. Mud is deposited through waning flow, whereas sand is periodically transported and deposited by traction currents. Occasionally, the environment of deposition was favorable for life, as indicated by the presence of burrowing and partially vegetated as indicated by the rootlets. The presence of mud cracks and extensive oxidized intervals suggest subaerial exposure (Walker, 1979).

The sharp, or undulating, bases and repeated alternation of sandstones and mudstones indicate high discharge flows entering a shallow-water environment, such as a small pond or playa-lake (Rogers and Astin, 1991; Clemmensen, 1998; Zhang et al., 1998). In well WWN-01, mudstones are mostly blue to grey suggesting mostly reducing, thus subaqueous conditions. In well BUM-01, the presence of hematite coatings around the sandstone grains, mud-crack structures, and gypsum/anhydrite nodules in the sandstones (Fig. 6e) indicates subaerial

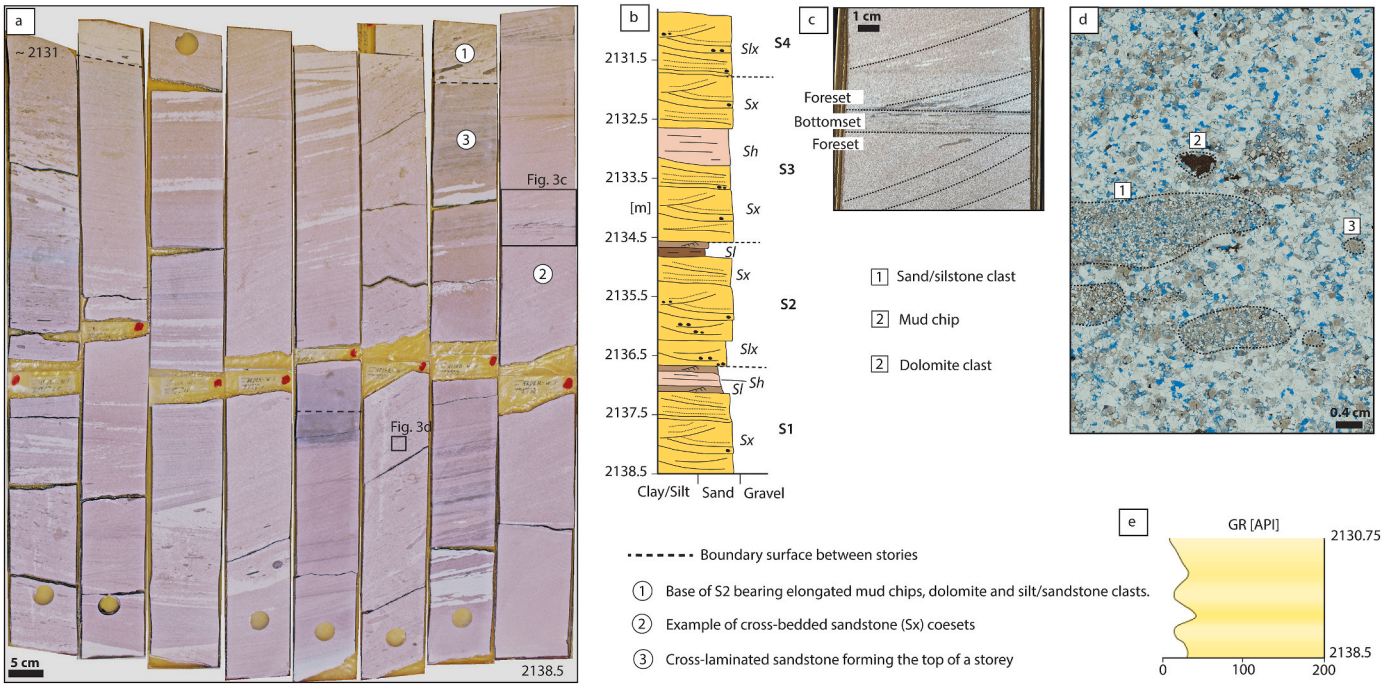

Fig. 3. Stacked stratified sandstone (LA-1). a) Example of LA-1 from well NDW-01 where dashed black lines represent the limit between storeys. b) Simplified sedimentary log displaying the succession of 3 storeys stacked on top of each other. Abbreviations are listed in Fig. 2. c) Bottomset foreset transition. See Fig. 3a for location. d) Example of texture and intraclasts from a pebbly sandstone (Slx). See Fig. 3a for location. e) Gamma ray profile of the core slabs displayed in Fig. 3a.

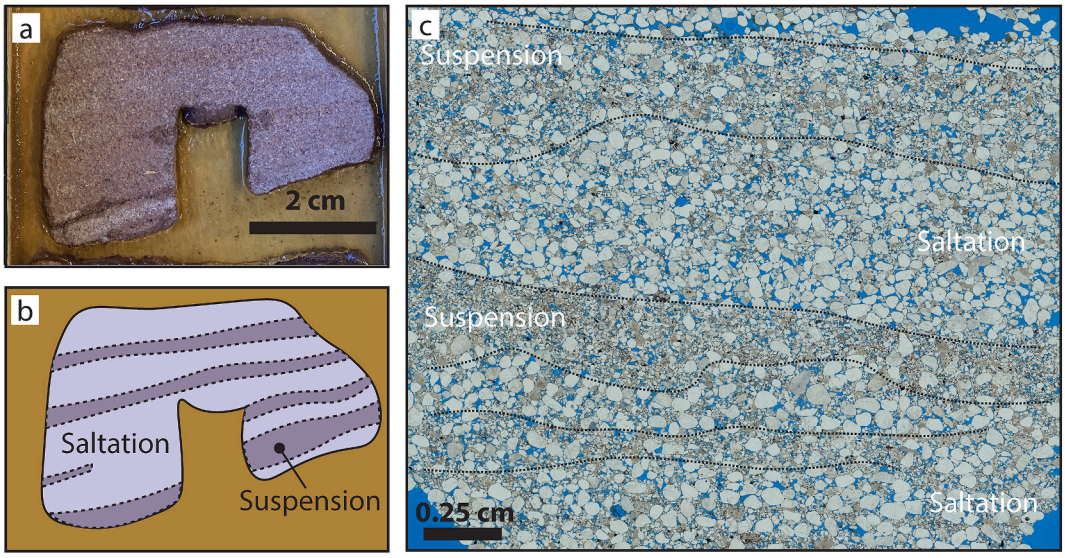

Fig. 4. Example of saltation and suspension deposited laminae from well NDW-01. a,b) Raw and interpreted core sample. c) Thin section from the sample in Fig. 4a. Pair of laminae where a lower well sorted laminae is deposited via saltation and an upper moderately sorted laminae is developed via suspension.

exposure, likely on arid mudflats (Zhang et al., 1998).

4.1.6. *Bioturbated and pedogenic mudstone (LA-6)*

This lithofacies association is characterized by a cm to m alternation of bioturbated and pedogenic claystone, siltstones, and sandy siltstone beds (Fig. 7a and b). Primary sedimentary structures are obscured, overprinted by the intense bioturbation and pedogenesis. Colour mottling is frequent with matrix colour ranging between reddish (5 YR 4/4) to greyish (GLEY 1 5/N). Burrows and rootlets represent the main type of bioturbation activity. Often, dolomite pedogenic nodules are present reaching 5–6 cm in size (Fig. 7a and c). On the gamma-ray, LA6 shows values above 120–130 API (Fig. 7d).

Interpretation: The lithofacies assemblage, fine grain size, and intercalation with LA-2 and LA-4 suggest deposition via suspension in a floodplain area. The absence of primary depositional structures, and the presence of bioturbation, colour mottling, and pedogenic nodules indicate soil-forming processes (Bourquin et al., 2009; Henares et al., 2020). The presence of dolomite nodules in the paleosol is likely related to precipitation under phreatic diagenetic conditions, with the incorporation of Mg into soil carbonate cement (Casado et al., 2014). These processes are enhanced in alkaline conditions in arid to semi-arid settings (Spötl and Wright, 2003). The presence of this lithofacies association on top of medium-grained cross-stratified sandstones (Sx) indicates that LA-6 could also form as mud plugs as a result of channel abandonment.

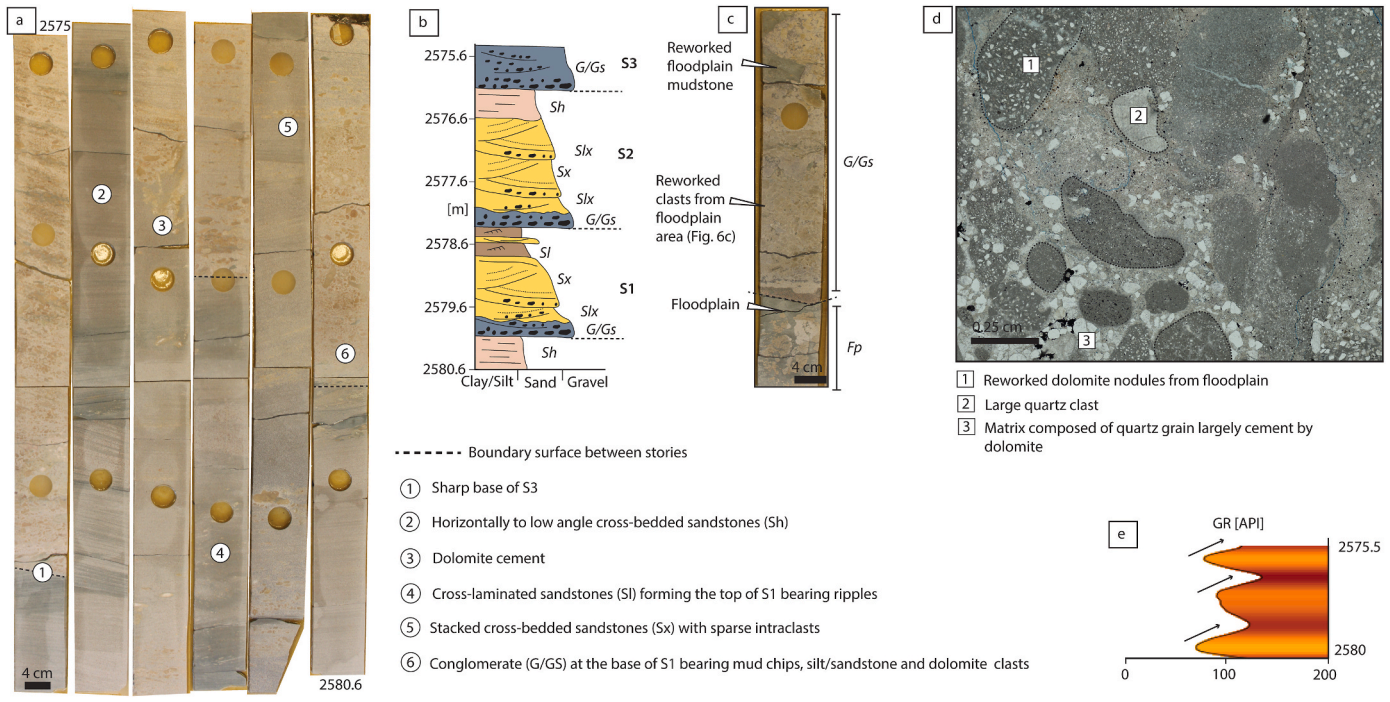

Fig. 5. Fining-upward sandstone (LA-2). a) Example of LA-2 from KWK-01 where dashed black lines represent the limit between storeys. b) Simplified sedimentary log displaying the succession of 3 storeys stacked on top of each other. Abbreviations are listed in Fig. 2. c) Example of gravel facies (G/Gs) overlying floodplain deposits showing soil development (Fp). d) Thin section from a gravel facies (G) from well KWK-01 at the depth of 2552.55 m. Note that most of the intraclasts are composed of dolomite. e) Gamma ray profile of the core slabs displayed in Fig. 5a.

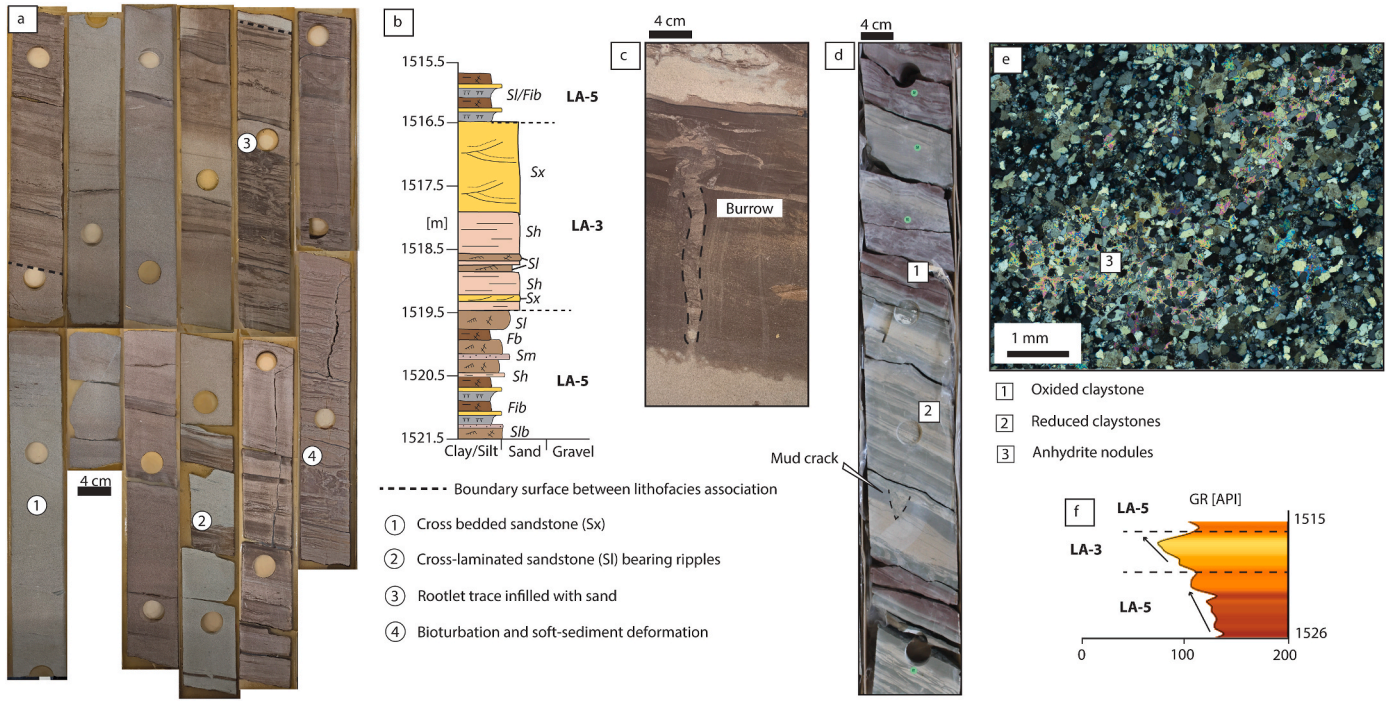

Fig. 6. Coarsening-upward sandstone (LA-3) and heterolithics (LA-5). a) Example of LA-3 and LA-5 from BUM-01 where dashed black lines represent the limit between the two lithofacies associations. b) Simplified sedimentary log displaying the succession of the two lithofacies associations. Abbreviations are listed in Fig. 2. c) Example of a bioturbated claystone (Fb) with a burrow (palaeophycus or planolites). d) Heterolithic interval from well WWN-01-S2. Note the presence of both grey (GLEY 16/5G) and red (2.5YR 4/2) indicating reduced and oxidized conditions respectively. e) Thin section from well BUM-01 at the depth 1502.2 m. The thin section shows the presence of anhydrite nodules. f) Gamma ray profile of the core slabs displayed in Fig. 6a.

4.2. Main Buntsandstein lithostratigraphy in the Roer Valley Graben

A lithostratigraphic correlation between wells is conducted to assess how lithofacies associations are distributed across the Roer Valley Graben and throughout the Main Buntsandstein Subgroup stratigraphy. First, the Main Buntsandstein Subgroup top and base boundaries have been identified in all the wells adopting the scheme proposed by Van Adrichem Boogaert and Kouwe (1993). The wells L02-01 and BUM-01 have been used as proxies (Fig. 10), as they record a typical Main Buntsandstein sedimentary section (Van Adrichem Boogaert and Kouwe, 1993). Following the same logic, the Main Buntsandstein Subgroup internal stratigraphic subdivision has been evaluated, and the lithofacies association distribution assessed.

4.2.1. Top and base Main Buntsandstein Subgroup

The Main Buntsandstein Subgroup is enclosed between the Lower Triassic Rogenstein Formation and the Upper Triassic Solling Formation (Van Adrichem Boogaert and Kouwe, 1993). In the Roer Valley Graben, the boundary with the Rogenstein Formation is marked by a sharp decrease in gamma-ray values from the claystones with oolite intercalations of the Rogenstein Formation (Palermo et al., 2000) with API values above ~120–130, to the sandstones of the Volpriehausen Formation with API values below ~70–80 (Fig. 10). This boundary is less pronounced in the southeastern part of the Roer Valley Graben (i.e. NDW-01 in Fig. 10) where the Rogenstein formation becomes more sandy (Palermo et al., 2000) and display lower average gamma ray values.

The upper boundary of the Main Buntsandstein is generally associated with the Hardegsen Unconformity in many basins across Europe (Bourquin et al., 2011). In the Roer Valley Graben, this unconformity has not been observed (Cecchetti et al., 2024) and the Hardegsen Formation appears to be conformably overlain by the Solling Formation, which has a gamma ray signature and sedimentary facies comparable to the underlying Hardegsen Formation. The Solling Formation in the Roer Valley Graben is composed of a 2–3 m thick lower sandy member (Basal Solling Sandstone Member) overlain by a ~10–20 m unit composed of silt/claystones interpreted as the Solling Claystone Member (Van Adrichem Boogaert and Kouwe, 1993). The sandstones from the Basal Solling Sandstone Member are stacked on top of the sandstones of the Hardegsen Formation, making the boundary between the Solling and Hardegsen Formations uncertain to define in the Roer Valley Graben. Thus, we decided to group the Basal Solling sandstones with the Hardegsen Formation (H + BSS in Fig. 10). This allows to take the top of the highest sandstone below the Solling Claystone Member as the marker of the top of the Main Buntsandstein Subgroup.

4.2.2. Main Buntsandstein Subgroup lithostratigraphy

The Volpriehausen and Detfurth Formations are each typically formed by a basal sandstone member and an upper claystone member (e.g. L02-01 in Fig. 10). In the proximal, southwestern part of the Roer Valley Graben, the Volpriehausen and Detfurth Formations form a continuous sandstone unit, composed of fluvial sandstones (LA-1) with gamma-ray values below ~70–80 API that reaches a maximum thickness of ~200 m in BKZ-01 (Fig. 10). Locally, silt-clay intercalations at dm to m scale cause gamma-ray values to increase up to ~100–110 API. The blocky profile on the gamma ray and the absence of significant claystone lithologies indicate that the claystone members are substituted by their sandy basin-fringe equivalent (Van Adrichem Boogaert and Kouwe, 1993). In this context, it is difficult to define formation boundaries given the prevalence of sandy lithologies. Thus, we have group the Volpriehausen and Detfurth Formations in the most proximal part of the Roer Valley Graben (VS + DS in Fig. 10).

In the distal sector of the Roer Valley Graben, a ~10–15 m interval of playa-lake (LA-5) sediments (VC2 in Fig. 10) seems to separate the Volpriehausen Formation from the Detfurth Formation and allows a tentative lithostratigraphic subdivision. In this area, the Volpriehausen

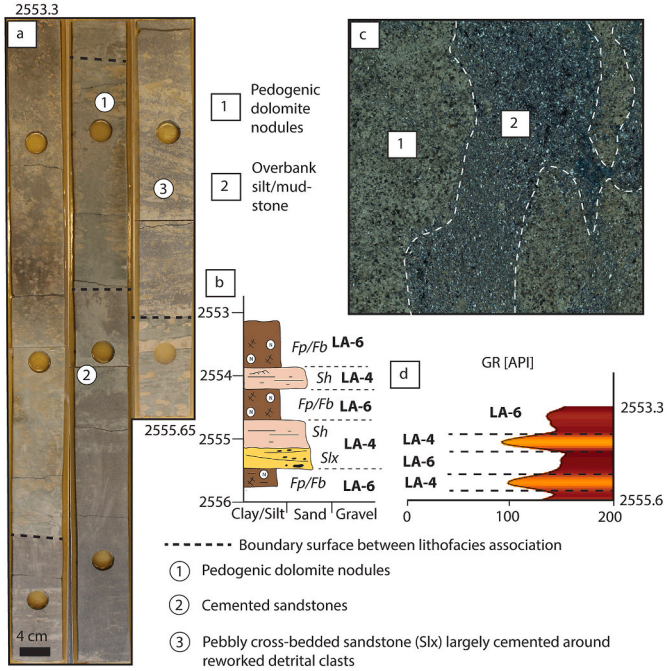

Fig. 7. Thin-bedded sandstone (LA-4) and bioturbated and pedogenic mudstone (LA-6). A) Example of LA-4 and LA-6 from KWK-01 where dashed black lines represent the limit between the two lithofacies associations. Abbreviations are listed in Fig. 2. B) Simplified sedimentary log displaying the succession of the two lithofacies associations. c) Thin section from well KWK-01 at the depth of 2581.55. The thin section shows pedogenic dolomite nodules in a pedogenic mudstone (Fp). D) Gamma ray profile of the core slabs displayed in Fig. 7a.

Formation ranges in total thickness between ~60 and ~75 m and is argued to be composed of two sandstone units (VS1 and VS2) with a generally blocky gamma ray profile and API values lower than ~90. These two sandstone units are largely composed of stacked stratified sandstones (LA-1) and show average thicknesses of ~25 m per unit across the distal area. In the northern part of the distal sector, the lithofacies association composition of the Volpriehausen Sandstone units changes. VS1 shows a bell profile on the gamma-ray suggesting fining-upward sandstones (LA-2), while VS2 shows a funnel-shape gamma ray profile indicating coarsening-upward sandstones (LA-3) (Fig. 10).

In the Roer Valley Graben, VS1 and VS2 are respectively overlain by a claystone interval that is defined here as the Volpriehausen Claystone unit (VC1 and VC2 in Fig. 10). The gamma-ray profile of the Volpriehausen Claystone units is formed by an alternation of peaks (>125 API) and troughs (100> API >125) readings. These peaks and troughs display similar profiles and values over a distance of ~500 m (e.g. WWN-01-S2 and WWN-02-S4 in Fig. 10). The two Volpriehausen Claystone units range from 10 to 15 m in thickness and display a general thickening from south to north. The transition from the Volpriehausen Claystone (VC1) to the Volpriehausen Sandstone (VS2) is generally gradual.

The character of the Volpriehausen Formation changes in the adjacent West Netherlands Basin and offshore the Netherlands (Fig. 10). In these areas, the Volpriehausen Formation is instead formed by the characteristic Main Buntsandstein Subgroup profile of a single basal sandstone of ~50 m in thickness and an upper claystone that reaches about 100 m offshore the Netherlands.

The Detfurth Formation has a blocky gamma-ray profile in the Roer Valley Graben and is largely composed of stacked fluvial sandstones (LA-1) with a total thickness that ranges from ~60 to 75 m (DS in Fig. 10). The dominance of sandy lithologies in the Roer Valley Graben seems to indicate that the Detfurth Claystone observed offshore the Netherlands is absent in this area and in the adjacent West Netherlands Basin

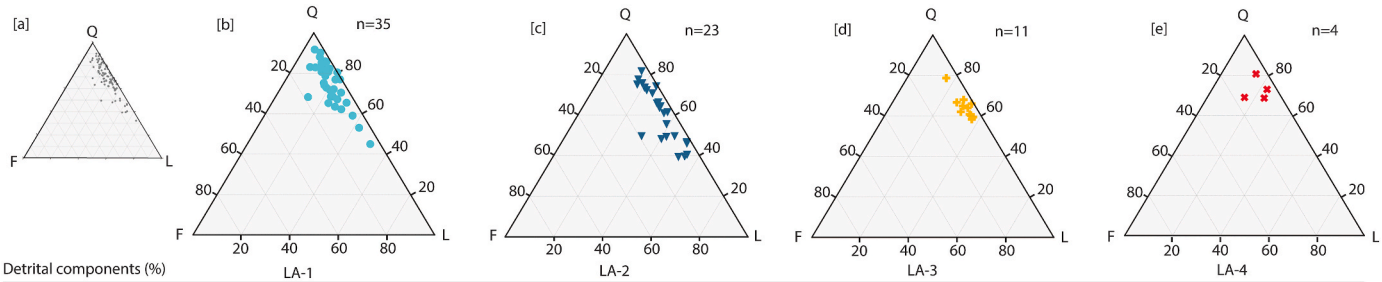

Detrital components (%)	LA-1	LA-2	LA-3	LA-4
Quartz	74.7	63.9	76.7	76.0
Feldspars	5.3	6.2	5.3	8.1
Silt/mudstone	10.3	19.2	16.4	13.8
Volcanic	< 0.1	0.5	< 0.1	< 0.1
Metamorphic	< 0.1	0.60	< 0.1	< 0.1
Dolomite	7	6	< 0.1	< 0.1
Chert	1.07	1.3	1.4	< 0.1
Mica	1.8	2.2	<0.1	2.1

Fig. 8. Detrital composition data of the sandy lithofacies associations. a) All thin section data. b) Detrital composition data of stacked stratified sandstone (LA-1). c) Detrital composition data of fining-upward sandstone (LA-2). d) Detrital composition data for coarsening-upward sandstone (LA-3). e) Detrital composition data for thin-bedded sandstone (LA-4).

(Fig. 10). To the north of the Roer Valley Graben, the average N/G of the Detfurth Formation decreases, and low gamma-ray readings (~70–80 API) are locally alternated with high gamma-ray (~140–150 API) intervals. These high gamma-ray intervals are on average 1–2 m thick, but they can reach 7–8 m (e.g. KWK-01 and BUM-01 in Fig. 10). Although it may be tentative to correlate these high gamma ray intervals with the Detfurth Claystone observed offshore the Netherlands, the absence of core data makes such correlation speculative.

The lower boundary between the Volpriehausen Claystone unit 2 (VC2) and the Detfurth Sandstone unit (DS) is generally characterized by a sharp decrease in gamma-ray readings from 160 to 170 API for the VC2 to ~60–70 API for the DS. This likely represents the fluvial system building out during the DS deposition while the playa-lake system retreats. To the north, the transition from VC2 to DS becomes gradual. The boundary between the Detfurth Formation and the overlying Hardegsen Formation is characterized by an increase in average gamma-ray of 40–50 API. This reflects the increase in claystone lithologies in the Hardegsen.

The Hardegsen Formation (H + BSS) is composed of an alternation of fluvial sandstones (LA-2), crevasse splays (LA-4), and paleosols (LA-6). The formation thickness ranges from ~25 to over 50 m in certain wells located in the proximal area (e.g. BKZ-01 in Fig. 10). It is distinguished from the underlying Detfurth Sandstone due to the lower N/G and the presence of paleosols. Fluvial sandstone units have on average values below ~80–90 API and can be stacked forming complexes up to ~9–10 m. These are embedded in claystone units with gamma-ray readings larger than ~110–120 API and thickness up to ~4–5 m.

5. Discussion

5.1. Regional depositional model

Three conceptual depositional models are proposed to explain the processes responsible for the deposition of the different lithofacies associations observed in the Main Buntsandstein Subgroup in the Roer Valley Graben (Fig. 11). The first two models represent depositional environments for the Volpriehausen and Detfurth Sandstone and Claystone units respectively, while the third represents depositional environment for the Hardegsen Formation.

5.1.1. Deposition of the Volpriehausen and Detfurth Sandstone units

The Volpriehausen and Detfurth Sandstone units are dominated by vertically-stacked fluvial sandstones representing deposition through high-energy, shallow rivers (Fig. 11a). The multistorey character, high degree of vertical amalgamation, lack of grain size trends, and high mobility of these channels suggest that these river systems were likely to be braided, as exemplified in many other adjacent Triassic basins (Ames and Farfan, 1996; Bourquin et al., 2007). The mobilization was likely enhanced by the presence of poorly consolidated banks due to the absence of vegetation and the sandy character of the interfluve environment (Steel and Thompson, 1983; Hassan et al., 2005; Gibling, 2006; Bourquin et al., 2009). The sandy interfluve environment was the locus for the formation of dolocrete, which subsequently was reworked and deposited within the channel sequences. This process is commonly observed in dryland systems (Molenaar and Felder, 2019) and, more particularly, in Triassic systems across northern European basins (Spötl and Wright, 2003; Schmid et al., 2006; Bertier et al., 2022).

Sediments in the Roer Valley Graben were sourced from the Variscan relicts as suggested by a regional decrease in N/G from south to north. This is in agreement with previous regional paleogeographic reconstruction at Germanic Basin scale (McKie and Williams, 2009; Bourquin et al., 2011; Olivarius et al., 2017). To the southeast, the Roer Valley Graben represented the gateway for the sediments from the Armorican and Rhenish Massifs to enter the Germanic basin. Once entered the Roer Valley Graben, rivers were likely flowing on average to NW, semi-parallel to the main fault trend (Cecchetti et al., 2024), like also suggested by the regional facies changes indicated by Geluk (2005) and paleoflow measurement indicators from borehole image logs (e.g., WWS-01). These long-drainage systems (~300–400 km) resulted in an overall high maturity of the sediments with a high degree of sorting, roundness, and a high percentage of quartz grains observed in the Roer Valley Graben.

The London-Brabant Massif was also a prominent structure during the Middle Triassic (Geluk et al., 2005; McKie and Williams, 2009). Considering its position and the half-graben setting, the London-Brabant Massif has likely contributed to feeding sediments to the Roer Valley Graben. From there, sediments were likely transported northwards by fluvial fan systems as suggested by Carter et al. (1990). However, these fan systems did likely not represent the major transport system in the Roer Valley Graben, Instead, they only represent a transverse zone located in the part proximal to the London-Brabant Massif feeding sediments to the major axial rivers flowing semi-parallel to the basin axis, a process commonly observed in half-graben settings (Gawthorpe and Leeder, 2000). The dominant NE-oriented axial fluvial transport agrees

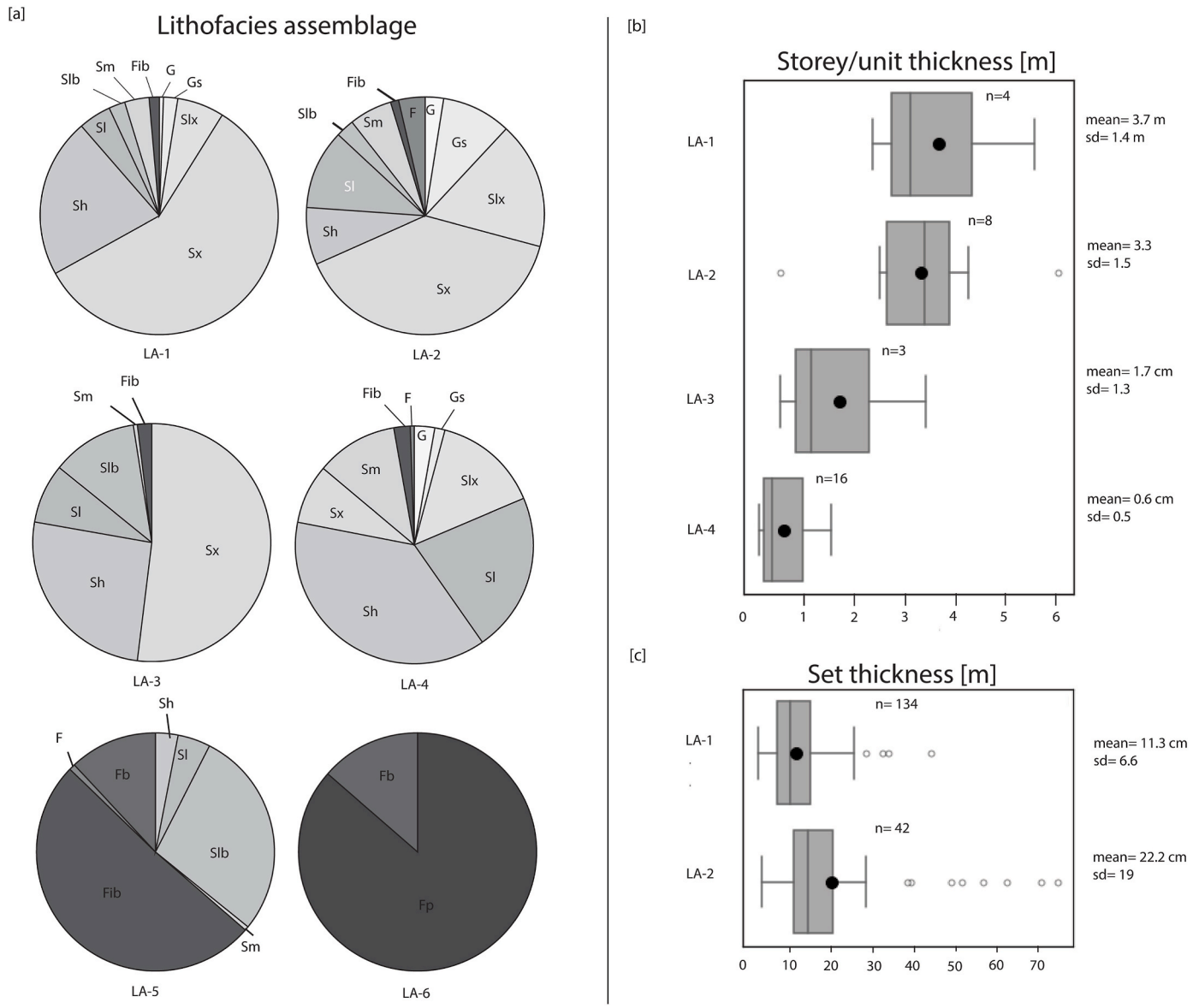

Fig. 9. a) Relative abundance of different lithofacies in each lithofacies association. Abbreviations are listed in Fig. 2. B) Sandstone thickness for the sandy lithofacies association. For LA-1 and LA-2 these values refer to each singular storey. For LA-3 and LA-4, these values refer to the thickness of the entire sandstone unit. c) Individual set thickness for LA-1 and LA-2.

with the larger paleogeographical setting, where sediments sourced from the distal Armorican Massif were transported along the Roer Valley Graben with an average northeast direction into the adjacent West Netherlands Basin and further to the north (e.g. Bachmann et al., 2010). Unfortunately, the erosion of Buntsandstein sediments along the northern margin of the London-Brabant Massif does not allow us to further investigate this model.

The Early to Middle Triassic was a period characterized by widespread arid to semi-arid conditions across the Germanic basin (Péron et al., 2005), with seasonal wetness enhanced by summer monsoons (Van der Zwan and Spaak, 1992). The very scarce presence of vegetation, absence of soil formation and sparse occurrence of aeolian sediments in the Volpriehausen and Detfurth Formations would support the rather arid climatic conditions. In the Roer Valley Graben, evidence of aeolian sedimentation has been found only in the southeastern part (Fig. 11a). The absence of aeolian sediments in the central part of the Roer Valley Graben may be related to the presence of basement massifs such as the London-Brabant Massif, acting as windshield and partly deflecting wind directions (Mader and Yardley, 1985) or simply the strong dominance of fluvial processes in the area given the proximity to the London-Brabant Massif source. Furthermore, the reductive colours of the fluvial sandstone in the north-west suggest more prolonged subaqueous conditions, thus less exposure to subaerial conditions and wind action. This could be the result of i) higher water discharge from the hinterland in relation to frequent precipitations during monsoon season (van der Zwan and Spaak, 1992); ii) shallower groundwater level considering the proximity to the recharge area; iii) the presence of faults located along the southern margin of the Roer Valley Graben (Cecchetti et al., 2024) potentially inducing upward water flow from the deeper aquifers (Verweij, 1993).

Along the northern flank of the Roer Valley Graben, the average low N/G indicates that the northern sector was an area subjected to sedimentation of fine-grained sediments (Cecchetti et al., 2024). The presence of terminal splays and fining-upward sandstones in BUM-01 suggests the northern sector to be the more distal and tectonically less active side of the basin. The occurrence of mud cracks and hematite-coated sediments indicate more frequent subaerial conditions than to the south where sandstones and claystones show reducing

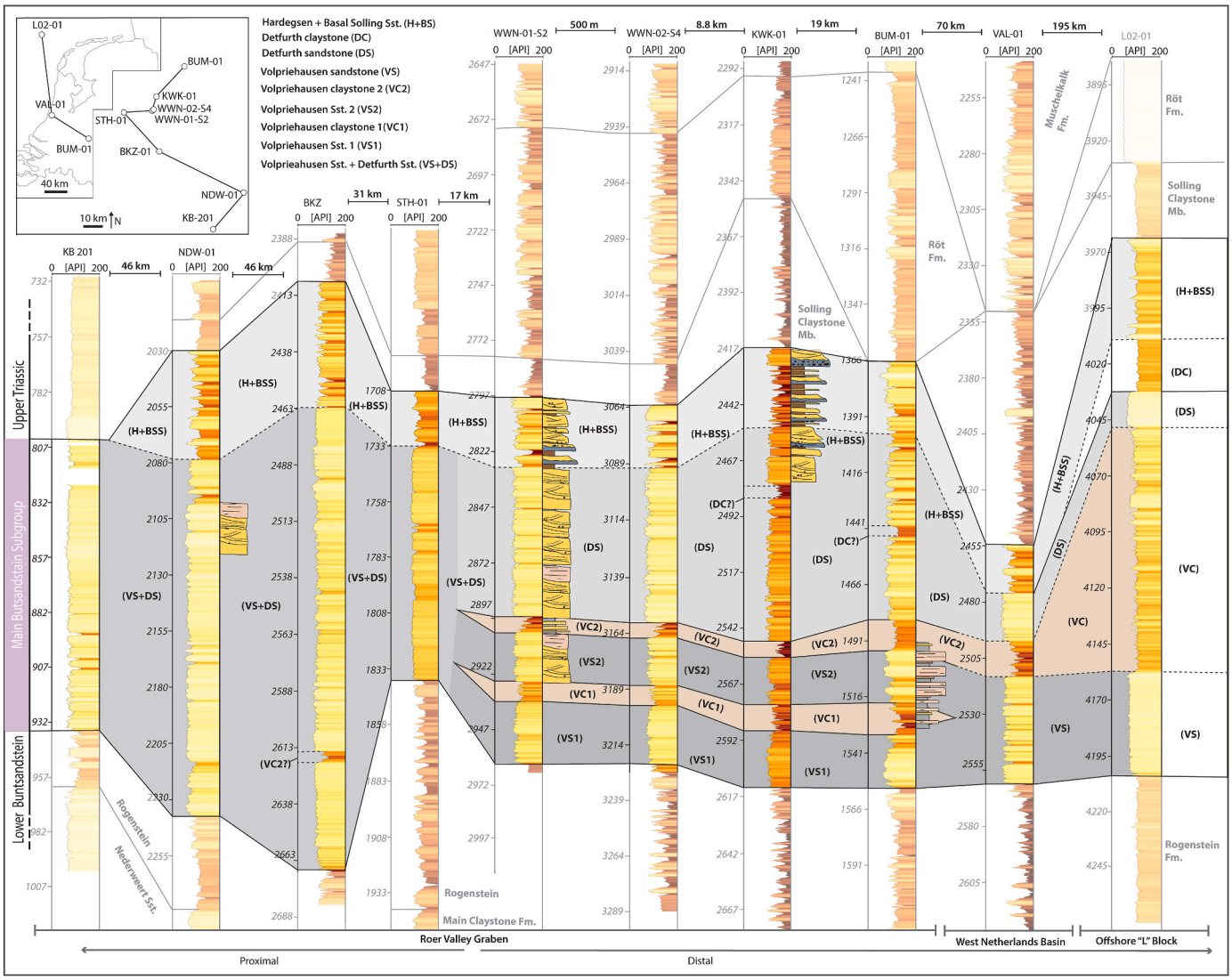

Fig. 10. Panel displaying the Buntsandstein lithostratigraphy across the study area. Well VAL-01 from the West Netherlands Basin and well L02-01 from offshore "L" block are included for regional correlation. The sedimentary logs are displayed next to the gamma-ray where core samples have been interpreted. See the text for full description.

colours. The exposure to subaerial conditions can be related to a slightly higher topographic position of the northern area of the Roer Valley Graben compared to its center. Therefore, the area was likely to be a floodplain area, periodically interested by fluvial sedimentation, but not an exposed high sourcing sediments to the adjacent basin. This is consistent with the regional setting and the presence to the north of the Central Netherlands Swell, a high topographic element during the Early to Middle Triassic times where only minor Buntsandstein sedimentation occurred (Geluk and Röhling, 1997). Unfortunately, the erosion of Lower Triassic sediments across the Roer Valley Graben flanks does not allow to further investigate this observation.

5.1.2. *Deposition of the Volpriehausen and Detfurth Claystone unit*

This model is representative for the deposition of ~10–15 m of playa-lake sediments in the central and northern part of the study area (Fig. 11b). The establishment of playa-lake conditions in the Roer Valley Graben is likely the product of repeated flash floods as a result of higher precipitation rates in the hinterland (Péron et al., 2005). The occurrence of oxidized and reduced mudstones indicates that sediments were exposed to both subaerial and subaqueous conditions. The presence of burrows and rootlets indicates that the environment was favorable for the formation of life. On average, the playa-lake claystones in the central part of the Roer Valley Graben show more reducing colours than in the northern part where sediments are largely oxidized. Thus, the water level was likely higher and more long-lasting in the central part of the Roer Valley Graben, while the northern sector was subjected to more frequent drainage (Fig. 11b). This can be a consequence of: i) shallower groundwater level closer to the London-Brabant Massif; ii) low topographic elevation induced by higher subsidence rates in the central part of the Roer Valley Graben creating a depression area where water accumulated.

Sands were periodically fed to the playa-lake through low-relief deltas as suggested by the coarsening-upward sandstone successions alternating with playa-lake sediments observed in the northern sector of the study area. The playa-lake sediments of the Volpriehausen Claystone units thin out and then disappear to the south (Fig. 10). The absence of playa-lake sediments along the southern margin of the Roer Valley Graben is likely dictated by the more proximal position in the basin, where sedimentation via fluvial processes was dominant. No clear evidence of the occurrence of Detfurth Claystone has been observed in the Roer Valley Graben, while this unit is present in the offshore sector of the Netherlands. This suggests that during the deposition of the Detfurth Formation, the Roer Valley Graben was an area subjected to fluvial activity, while playa-lake sedimentation was more restricted to the

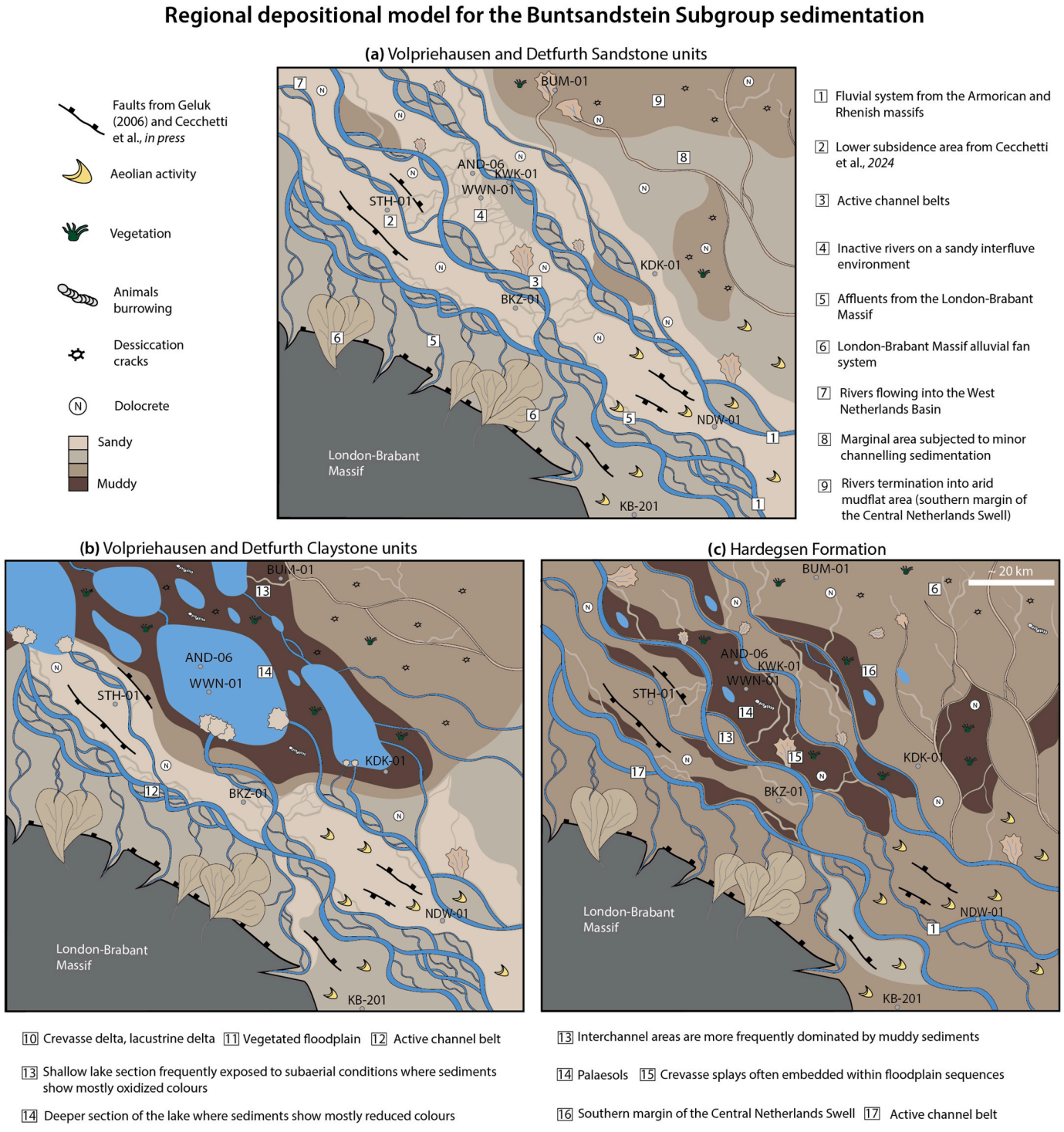

Fig. 11. Depositional model for the Main Buntsandstein in the study area. a) Depositional model for the deposition of the Volpriehausen and Detfurth Sandstone units in the study area. b) Depositional model for the deposition of the Volpriehausen and Detfurth claystone units. c) Depositional model for the deposition of the Hardegsen Formation.

northern distal area of the Netherlands (i.e. well L02-01 in Fig. 10)

The presence of similar playa-lake sedimentary structures and gamma-ray patterns in many wells across the Roer Valley Graben, the West Netherlands Basin, and other onshore and offshore basins in the Netherlands (Ames and Farfan, 1996; Kortekaas et al., 2018), indicates a large lateral extent of the same sedimentation conditions. The thickening of these sediments to the north (e.g. L02-01 in Fig. 10) suggests that playa-lake sedimentation was more pervasive and likely prolonged in the northern part of the Netherlands, while the Roer Valley Graben was more frequently interrupted by fluvial deposition. This is further supported by the presence of oolite and Avicula beds offshore in the Netherlands indicating the establishment of more perennial lacustrine conditions (Van Adrichem Boogaert and Kouwe, 1993).

5.1.3. Deposition of the Hardegsen Formation

This depositional model is representative for the upper part of the Buntsandstein stratigraphy, where the fining-upward nature of the fluvial sandstones, the preservation of overbank sediments and the development of paleosols indicate deposition via rivers that were more perennial and laterally stable than the rivers responsible for the deposition of the Volpriehausen and Detfurth Formations (Fig. 11c). The formation of soils with fine sediments and rootlets enhances the cohesivity of the banks, limiting channel breaching and frequent shifting across the river plain.

Nonetheless, the paleosols were frequently affected by periods of river erosion. This is indicated by the presence of scour deposits at the base of the sandstone bodies with large intraclasts reworked from the surrounding overbank areas. Frequent interbedded crevasse splays suggest water escaping the main channel, which subsequently may act as an avulsion site for the channel to migrate giving rise to a new active branch of the river system (Field, 2001).

The Hardegsen Formation may represent a period in time during which a less arid climate (Bourquin et al., 2011) and reduced tectonic activity (Geluk, 2005) enhanced the development of a more stable fluvial system in the Roer Valley Graben. A change in climatic conditions and fluvial style during the deposition of the Hardegsen has been reported in many Triassic basins (Bourquin et al., 2011 and references therein). Bourquin et al. (2009) observed paleosol development in the northern part of France at the top of the Buntsandstein, suggesting a decrease in aridity upwards through the Buntsandstein stratigraphy in northern France. Such a change in climate seems also to be reflected in a different fluvial style, with channels more laterally stable and with higher average sinuosity (Mader, 1982).

5.2. Reservoir architecture and sedimentary heterogeneities

The Buntsandstein Subgroup experienced significant burial up to 3–4 km (Cecchetti et al., 2024) that has partially deteriorated reservoir quality. An interplay of compaction and cementation processes resulted in an overall reduction of porosity and permeability (Zijerveld et al., 1992; Purvis and Okkerman, 1996; Mijnlieff, 2020; Bertier et al., 2022). Nonetheless, sandstones from the Main Buntsandstein Subgroup in certain wells across the southern part of the Netherlands (e.g. SPC-01) show porosities up to 20 % and permeability values over 250–300 mD (www.nlog.nl).

In the Roer Valley Graben, the main reservoirs in the Buntsandstein Subgroup occur in fluvial sandstones (LA-1 and LA-2). Terminal splay deposits in BUM-01 (LA-3) may represent an additional type of reservoir where these elements form stacked complexes as observed by McKie (2011) in the Skagerrak Formation in the Central North Sea, or form additional reservoir volume when directly connected to the main fluvial reservoirs. Fluvial sandstones yield the largest scatter in values with porosity ranging between 2.6 % and 19.2 % and permeability between 0.02 and 752 mD (Fig. 12). Overall LA-1 shows higher porosity and permeability values (av. 13 % and 109 mD) than LA-2 (av. 8.1 % and 2 mD). The porosity and permeability of terminal splay sandstones average with 15 % and 60 mD. We acknowledge that diagenesis has a large impact on the Buntsandstein reservoir quality (Purvis and Okkerman, 1996; Geluk, 2005; Mijnlieff, 2020). However, its effect on present-day reservoir quality is beyond the scope of this work that focuses on the reservoir architecture and the primary heterogeneities.

Each sandstone type developed its own reservoir architecture with its set of heterogeneities (Figs. 13–15) that will subsequently be discussed.

5.2.1. Reservoir architecture style: stacked amalgamated sandstones

This type of reservoir architecture is formed by stacked stratified fluvial sandstone bodies (LA-1) and mostly occurs in the Volpriehausen and Detfurth Formations. In the proximal area of the Roer Valley Graben, where the Volpriehausen and Detfurth Formations form a single sandstone unit (VS + DS in Fig. 10), the architecture of the reservoir interval is mainly represented by a single continuous sandstone unit of ~200 m in thickness. In the wells located across the distal part, this continuous sandstone unit splits into thinner (~30–60 m) sandstone units separated by the 10–15 m thick playa-lake units (LA-5) (Fig. 13a). These fine-grained playa-lake sediments seem to be laterally present over distances of ~20–30 km (Fig. 10) and are usually characterized by low permeability values (av. ~4 mD). Therefore, these playa-lake sediments, if continuous, can form an important heterogeneity at km scale, by compartmentalizing the reservoir units and hamper vertical fluid flow.

The lateral extent of the reservoir units could not be quantified based solely on the available data. The analysis dune-scale bedforms suggests a width in the order of ~1375 ± 1022.4 m for the active channel belts based on empirical relations (Bridge and Tye, 2000). This would be in agreement with the dimensions of ancient and present-day channel-belt dimensions in such arid to semi-arid endorheic basins (Gibling, 2006). Furthermore, Cecchetti et al. (2024) show how the Buntsandstein reflectors are laterally continuous over 5–10 km, which would support the presence of similar sedimentation conditions over such a scale. The connectivity of the sandstone bodies is also a function of N/G, where connectivity is usually greater than 90 % if N/G is above 30 % for randomly distributed sandstone objects (Larue and Hovadik, 2006). In the Roer Valley Graben, the Volpriehausen and Detfurth Formations show N/G largely above 30 %, especially in the proximal area where these two form a continuous sandstone unit (Cecchetti et al., 2024). Therefore, considering the high mobility of these channels, reflector continuity, and the N/G across the Roer Valley Graben, sandstone bodies are likely to be connected horizontally at km scale.

The permeability structure of stacked amalgamated sandstone reservoirs is partially driven by the lithofacies and grain size dependency of the sandstone bodies, with the average permeability value decreasing from coarse to finer lithofacies. Pebbly sandstones (Slx) have the highest average permeability and porosity, with means of ~56 mD and 13.4 % respectively (Fig. 13c). Cross-stratified (Sx) and horizontally-stratified sandstones (Sh) are the most abundant lithofacies in stacked amalgamated sandstones, thus they compose the core of the reservoir units. These two lithofacies have permeability means of ~90.5 and ~10 mD respectively, with standard deviations of ~30 and ~37 (Fig. 13b and c). Such a scatter of permeability values could be related to: i) rhythmic variation in grain size and sorting between foresets cross-laminae and bottomsets producing interstitial fluid-flow anisotropy (Fig. 13d) (McKinley et al., 2011); ii) different burial history in the basin resulting in diverse diagenesis-related heterogeneities. The rest of the lithofacies that compose the lower and middle part of the reservoir body have mean permeability values ranging between 0.1 and 10 mD and porosities between 7 and 12.5 %. At the scale of the individual sandstone bodies (Fig. 13b), fine-grained deposits that drape bar elements, or channel plugs represent the main heterogeneities that can behave as baffles. These elements are generally formed by an assemblage of bioturbated ripple cross-laminated sandstones (Sl) and homogeneous laminated claystone (F), which yield values of permeability below 0.1 mD (Fig. 13e).

5.2.2. Reservoir architecture style: compensational stacked sandstones

This reservoir architecture is mainly composed of fining-upward sandstones (LA-2) and mainly occurs in the Hardegsen Formation. However, this type of architecture can also be found in the Volpriehausen and Detfurth Formations along the northern margin of the Roer Valley Graben (e.g. BUM-01 in Fig. 10). The architecture is characterized by sandstone units that can reach vertical thicknesses of ~ 9–10 m and can be embedded in overbank sequences bearing paleosols up to 2–3 m thick that may lower the vertical connectivity of the reservoir units (Fig. 14a).

The common preservation of floodplain sediments results in N/G values generally below ~0.6/0.7 for the Hardegsen Formation. A more heterogenous lithology is also supported by the presence of disrupted reflectors over distances below 1 km and frequent amplitude contrasts (Cecchetti et al., 2024). This indicates a more uncertain sandstone connectivity over spacings of a few hundred meters and that preserved remnants of floodplain deposits may represent major boundaries to vertical fluid flow if these are laterally continuous. Nonetheless, when sufficiently permeable, crevasse sandstones (LA-5) can enlarge the recovery volume and help increase sandstone connectivity (Fig. 14b) (Larue and Hovadik, 2006; Colombera and Mountney, 2021).

Internally, the permeability structure of the sandstone units is less depositional fabric dependent compared to the stacked amalgamated sandstones (Fig. 14c). The coarser part of these sandstone bodies that is largely composed by gravel (G and Gs) and sandy lithofacies (Slx, Sx and Sm) have average permeability below 2.5 The average low values of porosity and permeability of these gravel elements is likely related to the abundant presence of dolomite cement in these sandstones. The cement is sourced from the detrital dolomite reworked as intraclasts from the adjacent floodplain (Fig. 14e), a process widely recognized in dryland systems (Henares et al., 2016; Molenaar and Felder, 2019). At the scale of the individual sandstone bodies, these dolomite-cemented units represent a heterogeneous layer that may act as baffle.

The rest of the sandy lithofacies assemblage that usually composes the upper part of the reservoir units has permeability means below 1 mD, with ripple cross-laminated sandstones (Sl) yielding the lowest average permeability of 0.2 mD (Fig. 14c). This may be associated with the alternation of finer and coarser grain size laminae, sorting and presence of small-scale micaceous laminae and rip-up clasts (Henares et al., 2020). Locally, as a result of channel abandonment, channel plugs can develop with bioturbated ripple cross-laminated sandstones and mudstones that may exhibit bioturbation (Fb) (Fig. 14d). The permeability of these elements is usually below 1 mD, thus they represent heterogeneities that can hamper flow.

5.2.3. Reservoir architecture style: marginal isolated sandstones

These reservoirs are composed of coarsening-up sandstones that can be stacked on top of each other reaching a total thickness of ~4/5 m (Fig. 15a). This type of reservoir has only been observed in the Volpriehausen Formation, but it is not excluded that it could be found in the other Buntsandstein formations along the northern margin of the Roer Valley Graben (Fig. 11) The architecture is characterized by sandstone units that are vertically separated by 5–15 m intervals of playa-lake sediments (LA-5) (Fig. 15a). Given the km-scale lateral extent of these playa-lake units, sandstone units are likely to be stratigraphically compartmentalized. However, cm-scale mud cracks and injection structures may form a network of vertical sandy pathways that can connect the main reservoir units to the sandy layers present in the playa-lake sediments and potentially enlarge the reservoir volume (Fig. 15c).

The lateral extent and connectivity could not be estimated based on the available data as this lithofacies has only been recognized in one well. Nonetheless, it can be expected that these types of deposits cover lateral extent from hundreds of meters up to several kilometers (Tooth, 2005; McKie and Audretsch, 2005; Fisher et al., 2008; Coronel et al., 2020)

The porosity and permeability of these sandstone bodies appear to be depositional facies controlled, with a general decrease of the average values from the coarser to the finer grain size fraction (Fig. 15e). The best reservoir quality is found in the coarser upper part of the coarsening-up sandstones composed by very fine to medium cross-stratified sandstones with an average permeability and porosity of ~75.8 mD and ~16.1 % and standard deviation of ~75. And 2.6 respectively. In the foresets, the coarser-grained laminae are usually better sorted and represent the more porous and permeable layers, while

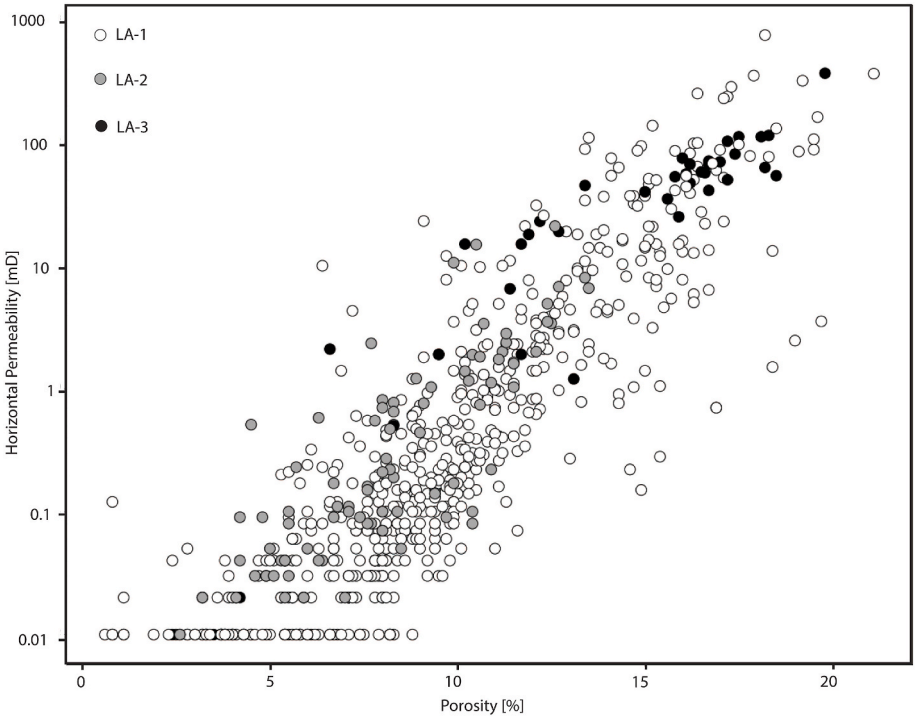

Fig. 12. Buntsandstein reservoir facies porosity and horizontal permeability from different wells in the Roer Valley Graben.

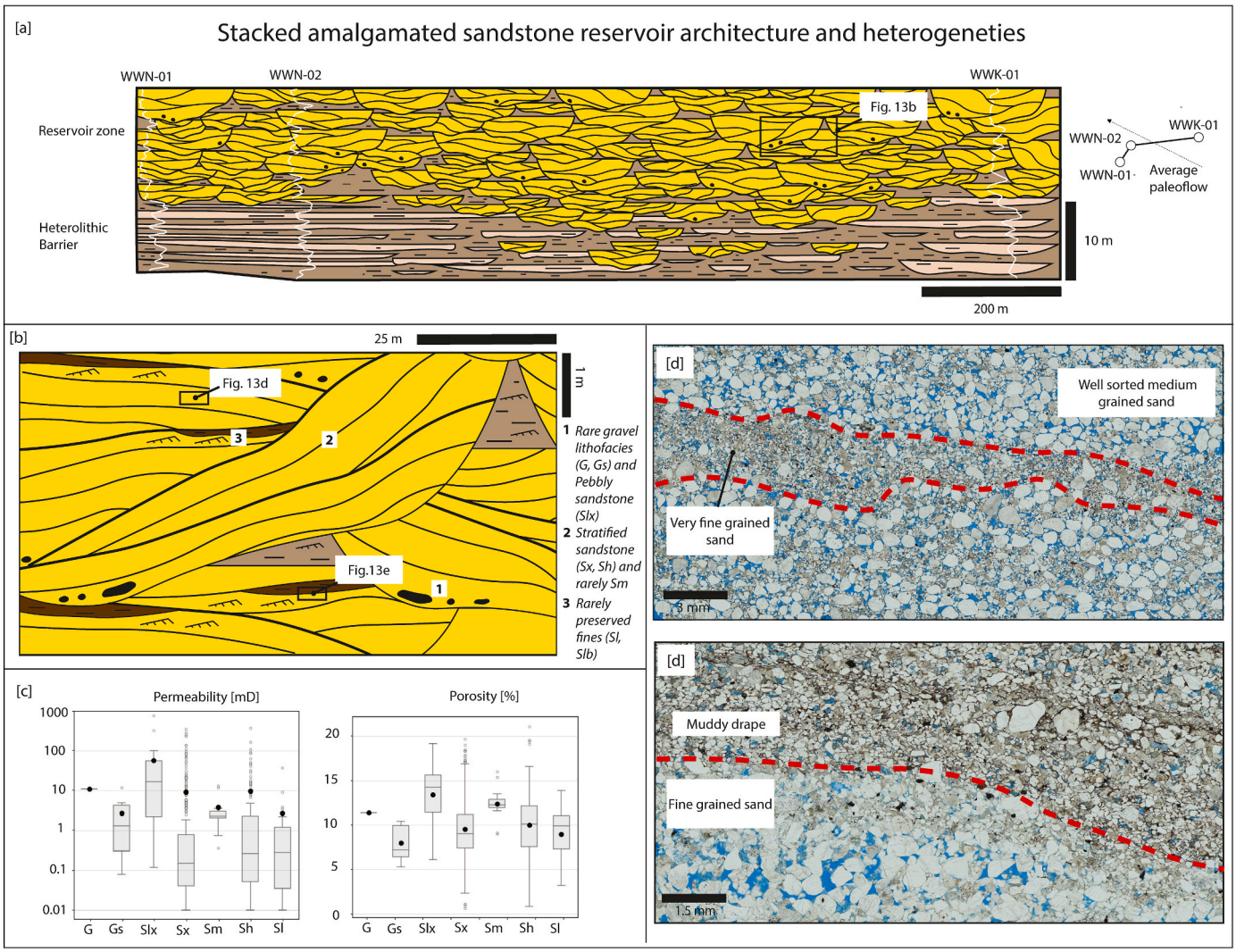

Fig. 13. Conceptual model representing architecture and sedimentary heterogeneities of stacked amalgamated sandstone reservoirs. a) Field-scale architecture with main reservoir bodies composed of stacked stratified sandstone bodies. The panel is semi-perpendicular to the average paleoflow direction. b) This figure represents the internal lithofacies assemblage and heterogeneities within LA-1. c) Boxplots displaying permeability and porosity of the main lithofacies occurring in this lithofacies association. The black dot represents the mean and the line within each box is the median. d) Typical example of sorting and grain size variation in the cross-stratified sandstones (Sx) that may result in preferential fluid pathways. Thin section from well NDW-01 at the depth of 2120.75 m. e) An example of vertical barrier where a mud drape overlies a fine-grained ripple cross-laminated sandstone. The thin section is from well NDW-01 at the depth of 2137.20 m.

the finer laminae have a worse sorting and higher clay content (Fig. 15e). Such structure will likely establish preferential flow pathways across the dip of the inclined laminae (Weber, 1982). The lower part of the complex where very fine to fine-grained, horizontally-stratified and ripple cross-laminated sandstones are dominant is characterized by a lower average permeability and porosity compared to the upper section, with minimum values of permeability and porosity that can reach 0.01 mD and 6 % respectively (Fig. 15e).

6. Conclusions

A comprehensive study of sedimentology and lithostratigraphy has shown that the Main Buntsandstein Subgroup in the Roer Valley Graben has been deposited through different fluvial processes with local aeolian reworking.

The Volpriehausen and Detfurth Formations are characterized by an alternation of amalgamated fluvial channel sediments, deposited through highly mobile ephemeral rivers, and playa-lake sediments. The playa-lake sediments are not present along the southern margin of the Roer Valley Graben, where, in fact, sandstones are stacked to form a continuous sandstone unit reaching thicknesses of ~200 m.

The Hardegsen Formation, which forms the upper part of the Buntsandstein Stratigraphy, is instead characterized by an alternation of fluvial channel sediments, deposited by less mobile and more perennial-like rivers, and overbank facies that show paleosol development.

We believe that such a change in sedimentary facies association across the Buntsandstein stratigraphy is related to a decrease of aridity in time and a decrease in tectonic activity upwards in the Buntsandstein stratigraphy, as observed in adjacent Triassic basins. Despite the presence of many common depositional features between our model and the models already available in the literature for the Roer Valley Graben area, the change in fluvial style across the Buntsandstein stratigraphy had not been documented before. This is a fundamental aspect as different depositional processes produce different types of reservoir architectures with their own set of heterogeneities.

In the Buntsandstein, we identified three main types of reservoir architecture. Stacked amalgamated sandstones are the product of highly mobile rivers and are composed of interconnected sandstones. These sandstone bodies show the highest average permeabilities and porosities. However, the distribution in grain size and sorting within the

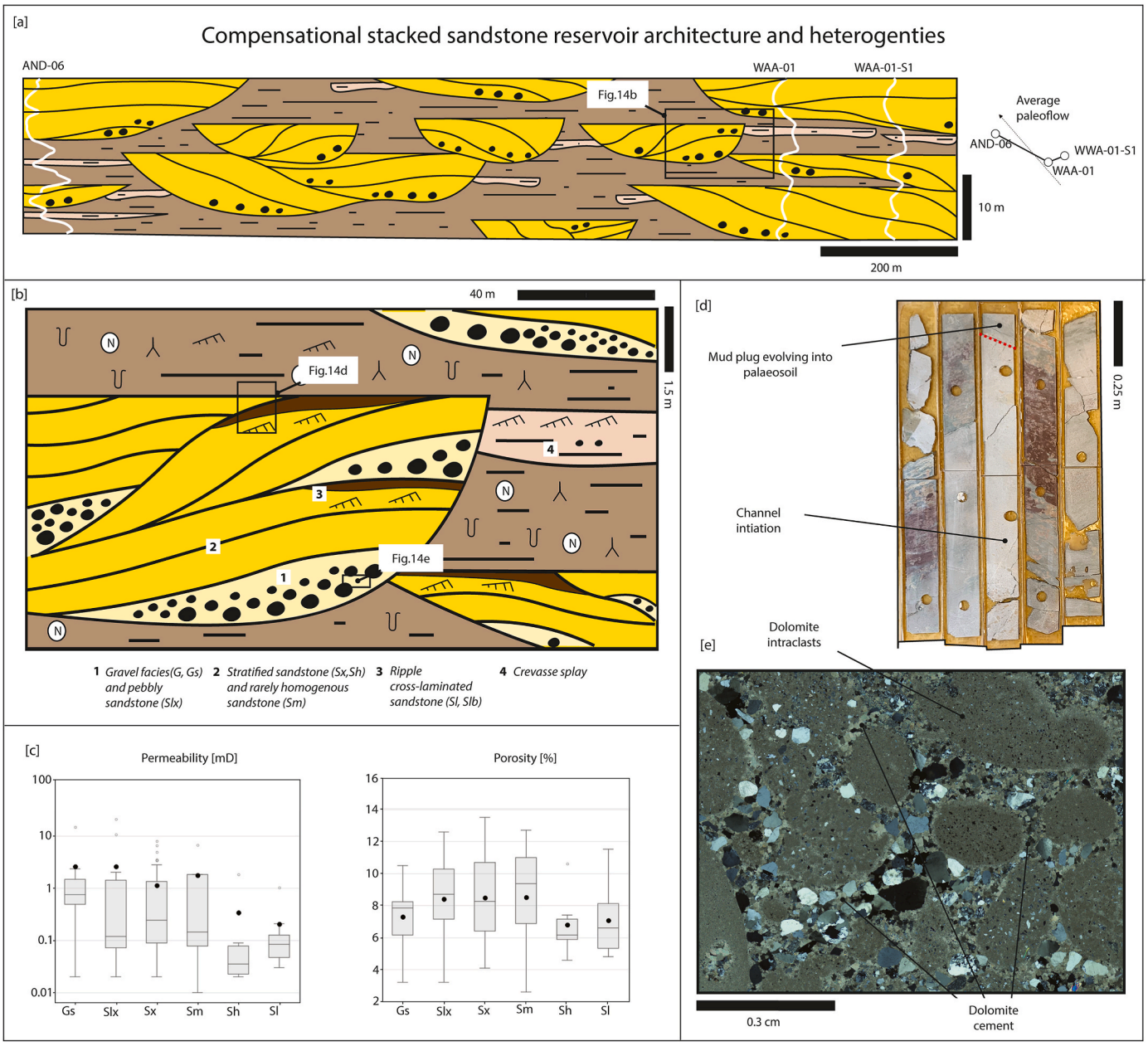

Fig. 14. Conceptual model representing architecture and sedimentary heterogeneities of stacked compensational sandstone reservoir. a) Field-scale architecture with main reservoir bodies composed of fining-upward sandstone bodies. Crevasse splays (LA-4) can locally help increasing overall connectivity and enlarge recovery volume. The panel is semi-parallel to the average paleoflow direction. b) This figure represents the internal lithofacies assemblage within LA-2. c) Boxplots displaying permeability and porosity of the main lithofacies occurring in this lithofacies association. The black dot represents the mean and the line within each box is the median. d) Sequence of sediments from well AND-06 displaying channel deposits subsequently plugged by bioturbated ripple cross-laminated sandstones evolving into paleosol above. e) Example of dolomite cemented gravel (G) where the dolomite intraclasts are sourced from the surrounding floodplains. The thin section is from well KWK-01 at the depth of 2552.55 m.

sandstones may result in uneven fluid flow. Compensational stacked sandstones form a reservoir architecture where sandstone bodies are less interconnected and a primary relationship with permeability and porosity seemed to have been altered by later diagenetic events. Within this architecture type, dolomite cemented intervals and mud plugs are important heterogeneities that may hamper fluid flow. The reservoir architecture composed of marginal isolated sandstone shows apparent preserved relationship between primary reservoir properties and depositional facies. The vertical connectivity of these sandstone bodies largely depends on the lateral extent of the heterolithic barriers.

CRediT authorship contribution statement

E. Cecchetti: Writing – review & editing, Writing – original draft, Visualization, Methodology, Investigation, Formal analysis, Data curation, Conceptualization. **A.W. Martinius:** Writing – review & editing, Supervision, Methodology, Investigation, Funding acquisition, Conceptualization, Writing – original draft. **M. Felder:** Writing – review & editing, Investigation. **M.E. Donselaar:** Writing – review & editing, Investigation. **H.A. Abels:** Writing – review & editing, Supervision, Methodology, Investigation, Funding acquisition, Conceptualization, Writing – original draft.

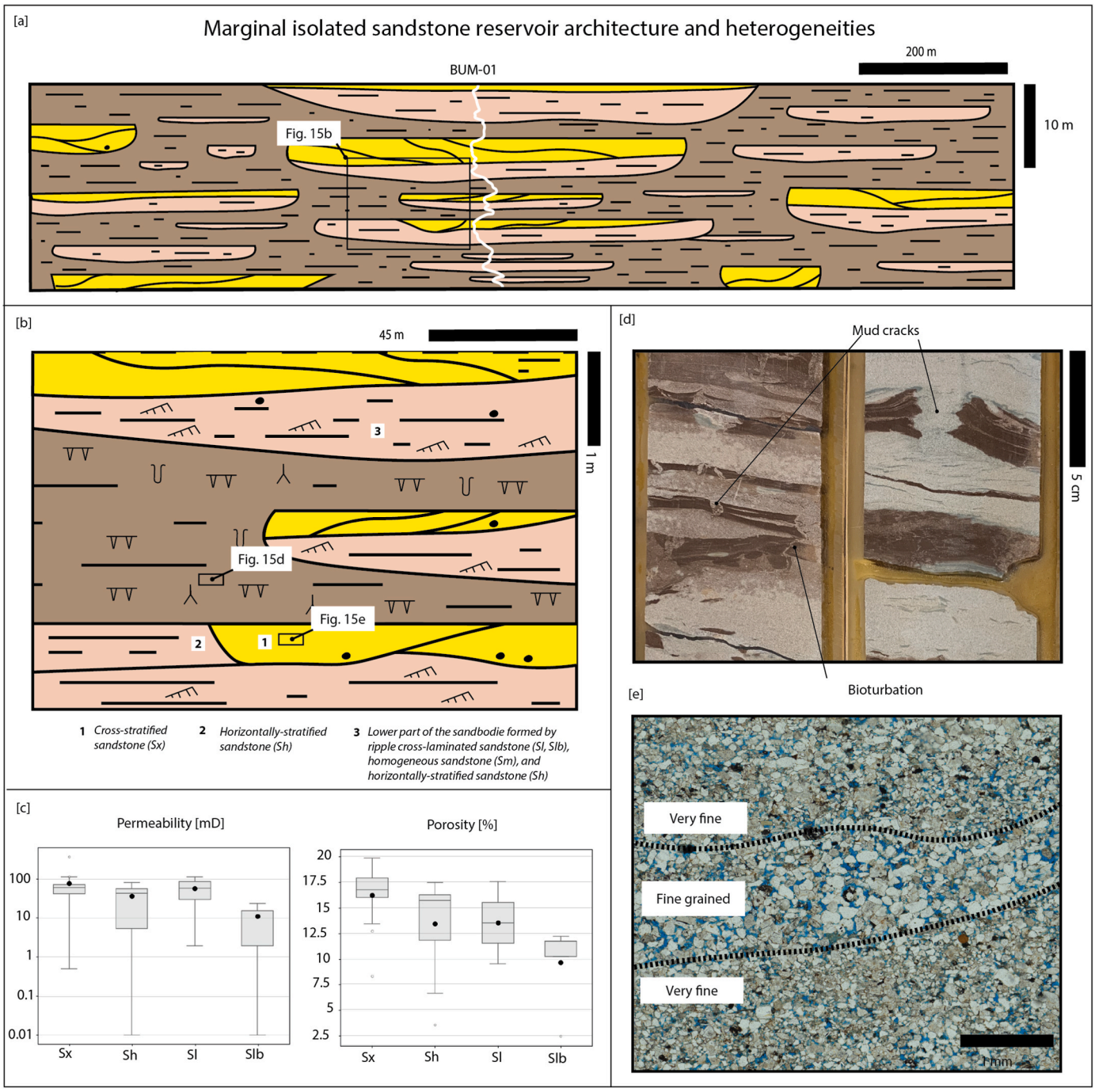

Fig. 15. Conceptual model representing architecture and heterogeneities of marginal isolated sandstone reservoir. a) Field-scale architecture, with main reservoirs composed of LA-3. b) This figure represents the internal lithofacies assemblage within LA-3. c) Boxplots displaying permeability and porosity of the main lithofacies occurring in this lithofacies association. The black dot represents the mean and the line within each box is the median. d) Core examples from well BUM-01 displaying extensive mud cracks and bioturbation that can connect the thin sandstone layers. e) Example of porosity and permeability variation between laminae with different grain size. The thin section is from well BUM-01 at the depth of 1502.2 m.

Declaration of competing interest

The authors declare that they have no known competing financial interests or personal relationships that could have appeared to influence the work reported in this paper.

Acknowledgments

The study is financially supported by Rijksdienst voor Ondernemend Nederland (RVO), Aardyn B.V. and PanTerra Geoconsultans B.V., Nederlandse Organisatie voor Toegepast Natuurwetenschappelijk Onderzoek (TNO), *Nederlandse Aardolie Maatschappij* (NAM)*, Wintershall Noordzee B.V. and Vermillion B.V. are thanked for providing access to the core material and thin sections. Particularly, our gratitude goes to* André Slupik *of TNO, and Clemens Visser, Rene Stoffers and Wiert Smit of NAM for sample access. Ewoud Hartemink is acknowledged for his contribution to the work during his MSc-thesis studies at TU Delft.* Thomas Voigt from Jena university is also acknowledged for his guidance during a fieldwork in the Triassic basins of the Thuringia area.

Data availability

Data will be made available on request.

References

Ames, R., Farfan, P.F., 1996. The environments of deposition of the Triassic main Buntsandstein Formation in the P and Q quadrants, offshore the Netherlands. In: Geology of Gas and Oil Under the Netherlands: Selection of Papers Presented at the 1983 International Conference of the American Association of Petroleum Geologists, Held in the Hague. Springer, Netherlands, pp. 167–178.

Bachmann, G.H., Geluk, M.C., Warrington, G., Becker-Roman, A., Beutler, G., Hagdorn, H., Hounslow, M.W., Nitsch, E., Rohling, H.G., Simon, T., Szulc, A., 2010. Triassic. In: Doornenbal, J.C., Stevenson, A.G. (Eds.), Petroleum Geological Atlas of the Southern Permian Basin Area. EAGE Publications b.v., Houten, pp. 149–173.

Bertier, P., Swennen, R., Kemps, R., Laenen, B., Dreesen, R., 2022. Reservoir characteristics and diagenesis of the Buntsandstein sandstones in the Campine Basin (NE Belgium). Geol. Belg. 25 (3–4), 145–184. https://doi.org/10.20341/gb.2022.004, 2022.

Bourquin, S., Peron, S., Durand, M., 2006. Lower Triassic sequence stratigraphy of the western part of the Germanic Basin (west of Black Forest): fluvial system evolution through time and space. Sediment. Geol. 186 (3–4), 187–211.

Bourquin, S., Durand, M., Diez, J.B., Broutin, J., Fluteau, F., 2007. The Permian-Triassic boundary and Early Triassic sedimentation in Western European basins: an overview. J. Iber. Geol. 33 (2), 221–236.

Bourquin, S., Guillocheau, F., Péron, S., 2009. Braided rivers within an arid alluvial plain (example from the Lower Triassic, western German Basin): recognition criteria and expression of stratigraphic cycles. Sedimentology 56 (7), 2235–2264.

Bourquin, S., Bercovici, A., López-Gómez, J., Diez, J.B., Broutin, J., Ronchi, A., Durand, M., Arché, A., Linol, B., Amour, F., 2011. The Permian–Triassic transition and the onset of Mesozoic sedimentation at the northwestern Peri-Tethyan domain scale: palaeogeographic maps and geodynamic implications. Palaeogeogr. Palaeoclimatol. Palaeoecol. 299 (1–2), 265–280.

Bradley, R.W., Venditti, J.G., 2017. Reevaluating dune scaling relations. Earth Sci. Rev. 165, 356–376.

Bridge, J.S., 2006. Fluvial facies models: recent developments. In: Posamentier, H., Walker, R.G. (Eds.), Facies Models Revisited, 84. SEPM Spec. Publ., pp. 85–170

Bridge, J.S., Tye, R.S., 2000. Interpreting the dimensions of ancient fluvial channel bars, channels, and channel belts from wireline-logs and cores. AAPG Bull. 84 (8), 1205–1228.

Bryant, M., Falk, P., Paola, C., 1995. Experimental study of avulsion frequency and rate of deposition. Geology 23 (4), 365–368.

Buatois, L.A., Mángano, M.G., 1998. Trace fossil analysis of lacustrine facies and basins. Palaeogeogr. Palaeoclimatol. Palaeoecol. 140 (1–4), 367–382.

Busch, B., Adelmann, D., Herrmann, R., Hilgers, C., 2022. Controls on compactional behavior and reservoir quality in a Triassic Buntsandstein reservoir, Upper Rhine Graben, SW Germany. Mar. Petrol. Geol. 136, 105437.

Cain, S.A., Mountney, N.P., 2009. Spatial and temporal evolution of a terminal fluvial fan system: the Permian organ rock Formation, South-east Utah, USA. Sedimentology 56 (6), 1774–1800.

Carter, R., Cade, C., Amiri Garoussi, K., 1990. Sedimentology and reservoir quality of the middle and upper bunter formations, cores 1-7 Waalwijk-2. EXT, 58541.

Casado, A.I., Alonso-Zarza, A.M., La Iglesia, Á., 2014. Morphology and origin of dolomite in paleosols and lacustrine sequences. Examples from the Miocene of the Madrid Basin. Sediment. Geol. 312, 50–62.

Cecchetti, E., Martinius, A., Bruna, P.O., Bender, A., Abels, H., 2024. Structural controls on the main Buntsandstein sediment distribution in the Roer Valley Graben. the Netherlands. Submitted to Neth. J. Geosci.

Clemmensen, L.B., 1998. Desert Sand Plain and Sabkha Deposits from the Bunter Sandstone Formation (L. Triassic) at the northern margin of the German Basin. Geol. Rundsch. 74 (3), 519–536.

Colombera, L., Mountney, N.P., 2021. Influence of fluvial crevasse-splay deposits on sandbody connectivity: lessons from geological analogues and stochastic modelling. Mar. Petrol. Geol. 128, 105060.

Coronel, M.D., Isla, M.F., Veiga, G.D., Mountney, N.P., Colombera, L., 2020. Anatomy and facies distribution of terminal lobes in ephemeral fluvial successions: jurassic Tordillo Formation, Neuquén Basin, Argentina. Sedimentology 67 (5), 2596–2624.

Donselaar, M.E., Cuevas Gozalo, M.C., van Toorenenburg, K.A., Wallinga, J., 2022. Spatio-temporal reconstruction of avulsion history at the terminus of a modern dryland river system. Earth Surf. Process. Landf. 47 (5), 1212–1228.

Field, J., 2001. Channel avulsion on alluvial fans in southern Arizona. Geomorphology 37 (1–2), 93–104.

Fielding, C.R. and Crane, R.C., 1987. An application of statistical modelling to the prediction of hydrocarbon recovery factors in fluvial reservoir sequences.

Fielding, C.R., 2006. Upper flow regime sheets, lenses and scour fills: extending the range of architectural elements for fluvial sediment bodies. Sediment. Geol. 190 (1–4), 227–240.

Fisher, J.A., Nichols, G.J., Waltham, D.A., 2007. Unconfined flow deposits in distal sectors of fluvial distributary systems: examples from the Miocene Luna and Huesca systems, northern Spain. Sediment. Geol. 195 (1–2), 55–73.

Fisher, J.A., Krapf, C.B., Lang, S.C., Nichols, G.J., Payenberg, T.H., 2008. Sedimentology and architecture of the douglas creek terminal splay, Lake eyre, central Australia. Sedimentology 55 (6), 1915–1930.

Folk, R.L., Ward, W.C., 1957. Brazos river bar [texas]; a study in the significance of grain size parameters. J. Sediment. Res. 27 (1), 3–26.

Gawthorpe, R.L., Leeder, M.R., 2000. Tectono-sedimentary evolution of active extensional basins. Basin Res. 12 (3-4), 195–218.

Geluk, M.C., 2005. Stratigraphy and Tectonics of Permo-Triassic Basins in the Netherlands and Surrounding Areas. PhD Thesis. Utrecht University, Utrecht.

Geluk, M.C., Röhling, H.G., 1997. High-resolution sequence stratigraphy of the Lower Triassic 'Buntsandstein' in the Netherlands and northwestern Germany. Geol. Mijnbouw 76, 227–246.

Gibling, M.R., 2006. Width and thickness of fluvial channel bodies and valley fills in the geological record: a literature compilation and classification. J. Sediment. Res. 76 (5), 731–770.

Gómez-Gras, D., Alonso-Zarza, A.M., 2003. Reworked calcretes: their significance in the reconstruction of alluvial sequences (Permian and Triassic, Minorca, Balearic Islands, Spain). Sediment. Geol. 158 (3–4), 299–319.

Hartkamp-Bakker, C.A., Donselaar, M.E., 1993. Permeability patterns in point bar deposits: Ter-tiary Loranca Basin, central Spain. In: Flint, S.S., Bryant, I.D. (Eds.), The Geological Modelling of Hydrocarbon Reservoirs and Outcrop Analogues. Spec. Publ. Int. Assoc. Sediment. 15, pp. 157–168.

Hartmann, D.J., Beaumont, E.A., Foster, N.H., 1999. Predicting reservoir system quality and performance. Exploring for oil and gas traps: AAPG treatise of petroleum geology. Handb. Petrol. Geol. 9, 1.

Hassan, M.A., Church, M., Lisle, T.E., Brardinoni, F., Benda, L., Grant, G.E., 2005. Sediment transport and channel morphology of small, forested streams 1. Jawra J. Am. Water Resour. Assoc. 41 (4), 853–876.

Henares, S., Caracciolo, L., Cultrone, G., Fernández, J., Viseras, C., 2014. The role of diagenesis and depositional facies on pore system evolution in a Triassic outcrop analogue (SE Spain). Mar. Petrol. Geol. 51, 136–151.

Henares, S., Arribas, J., Cultrone, G., Viseras, C., 2016. Muddy and dolomitic rip-up clasts in Triassic fluvial sandstones: origin and impact on potential reservoir properties (Argana Basin, Morocco). Sediment. Geol. 339, 218–233.

Henares, S., Donselaar, M.E., Caracciolo, L., 2020. Depositional controls on sediment properties in dryland rivers: influence on near-surface diagenesis. Earth Sci. Rev. 208, 103297.

Herbert, C.M., Alexander, J., 2018. Bottomset architecture formed in the troughs of dunes and unit bars. J. Sediment. Res. 88 (4), 522–553.

Hjuler, M.L., Olivarius, M., Boldreel, L.O., Kristensen, L., Laier, T., Mathiesen, A., Nielsen, C.M., Nielsen, L.H., 2019. Multidisciplinary approach to assess geothermal potential, Tønder area, North German Basin. Geothermics 78, 211–223.

IF Technology, 2012. Geothermal Energy Noord-Brabant. Geological Study of Triassic Reservoirs in the Province of Noord-Brabant. 3/60125/NB.

Kombrink, H., Doornenbal, J.C., Duin, E.J.T., Den Dulk, M., Van Gessel, S.F., ten Veen, J. H., Witmans, N., 2012. New insights into the geological structure of the Netherlands; results of a detailed mapping project. Neth. J. Geosci. 91–4, 419–446. https://doi.org/10.1017/S0016774600000329.

Kortekaas, M., Böker, U., Van Der Kooij, C., Jaarsma, B., 2018. Lower Triassic reservoir development in the northern Dutch offshore. Geological Society, London, Special Publications 469 (1), 149–168.

Kramers, L., Van Wees, J.D., Pluymaekers, M.P.D., Kronimus, A., Boxem, T., 2012. Direct heat resource assessment and subsurface information systems for geothermal aquifers: the Dutch perspective. Netherlands J. Geosci./Geologie en Mijnbouw 91 (4), 637–649. https://doi.org/10.1017/S0016774600000421.

Larue, D.K., Hovadik, J.M., 2006. Connectivity of channelized reservoirs: a modelling approach. Pet. Geosci. 12, 291–308.

Leclair, S.F., Bridge, J.S., 2001. Quantitative interpretation of sedimentary structures formed by river dunes. J. Sediment. Res. 71 (5), 713–716.

Limaye, A.B., 2020. How do braided rivers grow channel belts? J. Geophys. Res.: Earth Surf. 125 (8), e2020JF005570.

Mackey, S.D., Bridge, J.S., 1995. Three-dimensional model of alluvial stratigraphy; theory and applications. J. Sediment. Res. 65 (1b), 7–31.

Mader, D., 1982. Aeolian sands in continental red beds of the Middle Buntsandstein (Lower Triassic) at the western margin of the German Basin. Sediment. Geol. 31 (3–4), 191–230.

Mader, D., Yardley, M.J., 1985. Migration, modification and merging in aeolian systems and the significance of the depositional mechanisms in Permian and Triassic dune sands of Europe and North America. Sediment. Geol. 43 (1–4), 85–218.

McKie, T., Williams, B., 2009. Triassic palaeogeography and fluvial dispersal across the northwest European Basins. Geol. J. 44 (6), 711–741.

McKie, T., 2011. Architecture and behavior of dryland fluvial reservoirs , Triassic Skagerrak Formation, Central North Sea. In: Davidson, S.K., Leleu, S., North, C.P. (Eds.), From River to Rock Record: the Preservation of Fluvial Sediments and Their Subsequent Interpretation, 97. SEPM Special Publication, pp. 189–214. https://doi.org/10.2110/sepmsp.097.189.

McKie, T. and Audretsch, P., 2005. Depositional and structural controls on Triassic reservoir performance in the Heron Cluster, ETAP, Central North Sea.

McKinley, J.M., Atkinson, P.M., Lloyd, C.D., Ruffell, A.H., Worden, R.H., 2011. How porosity and permeability vary spatially with grain size, sorting, cement volume, and mineral dissolution in fluvial Triassic sandstones: the value of geostatistics and local regression. J. Sediment. Res. 81 (12), 844–858.

Miall, A.D., 1977. A review of the braided-river depositional environment. Earth Sci. Rev. 13 (1), 1–62.

Miall, A.D., 1981. Facies models for alluvial fans and braided rivers. In: Walker, R.G. (Ed.), Facies Models, first ed. Geoscience Canada, pp. 189–213.

Mijnlieff, H.F., 2020. Introduction to the geothermal play and reservoir geology of the Netherlands. Netherlands J. Geosci. 99, e2. https://doi.org/10.1017/njg.2020.2.

Molenaar, N., Felder, M., 2019. Origin and distribution of dolomite in Permian Rotliegend siliciclastic sandstones (Dutch Southern Permian Basin). J. Sediment. Res. 89 (10), 1055–1073.
Morad, S., Al-Ramadan, K., Ketzer, J.M., De Ros, L.F., 2010. The impact of diagenesis on the heterogeneity of sandstone reservoirs: a review of the role of depositional facies and sequence stratigraphy. AAPG Bull. 94 (8), 1267–1309.
Mountney, N.P., Thompson, D.B., 2002. Stratigraphic evolution and preservation of aeolian dune and damp/wet interdune strata: an example from the Triassic Helsby Sandstone Formation, Cheshire Basin, UK. Sedimentology 49 (4), 805–833.
Nichols, G.J., Fisher, J.A., 2007. Processes, facies and architecture of fluvial distributary system deposits. Sediment. Geol. 195 (1–2), 75–90.
Nichols, G., 2009. Sedimentology and Stratigraphy, second ed. John Wiley & Sons, Chichester.
NITG, 2004. Geological Atlas of the Subsurface of the Netherlands – Onshore. Netherlands Institute of Applied Geoscience TNO (Utrecht), p. 104.
North, C.P., Taylor, K.S., 1996. Ephemeral-fluvial deposits: integrated outcrop and simulation studies reveal complexity. AAPG Bull. 80 (6), 811–830.
Olivarius, M., Weibel, R., Friis, H., Boldreel, L.O., Keulen, N., Thomsen, T.B., 2017. Provenance of the Lower Triassic Bunter Sandstone Formation: implications for distribution and architecture of aeolian vs. fluvial reservoirs in the North German Basin. Basin Res. 29, 113–130.
Palermo, D., Aigner, T., Geluk, M., Pöppelreiter, M., Pipping, K., 2008. Reservoir potential of a lacustrine mixed carbonate/siliciclastic gas reservoir: the Lower Triassic Rogenstein in the Netherlands. J. Petrol. Geol. 31 (1), 61.
Parkash, B., Awasthi, A.K., Gohain, K., 1983. Lithofacies of the Markanda terminal fan, Kurukshetra district, Haryana, India. In: Collinson, J.D., Lewin, J. (Eds.), Modern and Ancient Fluvial Systems, 6. International Association of Sedimentologists Special Publication, pp. 337–344.
Péron, S., Bourquin, S., Fluteau, F., Guillocheau, F., 2005. Paleoenvironment reconstructions and climate simulations of the Early Triassic: impact of the water and sediment supply on the preservation of fluvial systems. Geodin. Acta 18 (6), 431–446.
Pettijohn, F.J., 1975. Sedimentary Rocks, 3. Harper & Row, New York, p. 628.
Pimentel, N.L., Wright, V.P., Azevedo, T.M., 1996. Distinguishing early groundwater alteration effects from pedogenesis in ancient alluvial basins: examples from the Palaeogene of southern Portugal. Sediment. Geol. 105 (1–2), 1–10.
Postma, G., 2014. Generic autogenic behavior in fluvialsystems: lessons from experimental studies. In: Martinius, A.W., Ravnas, R., Howell, J.A., Steel, R.J., &Wonham, J.P. (Eds.), From Depositional Systems to Sedimentary Successions on the Norwegian Continental Margin, 46. International Association of Sedimentologists, Special Publications, pp. 1–18.
Purvis, K., Okkerman, J.A., 1996. Inversion of reservoir quality by early diagenesis: an example from the Triassic Buntsandstein, offshore the Netherlands. In: Rondeel, H. E., Batjes, D.A.J., Nieuwenhuijs, W.H. (Eds.), Geology of Gas and Oil Under the Netherlands, pp. 179–189.
Ringrose, P.S., Martinius, A.W., Alvestad, J., 2008. Multiscale geological reservoir modelling in practice. Geol. Soc. 309 (1), 123–134. London, Special Publications.
Rogers, D.A., Astin, T.R., 1991. Ephemeral lakes, mudpellet dunes and wind-blown sand and silt: reinterpretations of Devonian lacustrine cycles in north Scotland. In: Anadon, P., Cabrera, L., Kelts, K. (Eds.), LacustrineFacies Analysis. Int. Assoc. Sedimentol. Spec. Publ., 13,199–222.
Sambrook Smith, G.H., Ashworth, P.J., Best, J.L., Woodward, J., Simpson, C.J., 2006. The sedimentology and alluvial architecture of the sandy braided South Saskatchewan River, Canada. Sedimentology 53 (2), 413–434.
Scheck, M., Bayer, U., 1999. Evolution of the Northeast German Basin—Inferences from a 3D structural model and subsidence analysis. Tectonophysics 313 (1–2), 145–169.
Schmid, S., Worden, R.H., Fisher, Q.J., 2006. Sedimentary facies and the context of dolocrete in the Lower Triassic Sherwood sandstone group: corrib field west of Ireland. Sediment. Geol. 187 (3–4), 205–227.
Spötl, C., Wright, V.P., 2003. Groundwater dolocretes from the Upper Triassic of the Paris Basin, France: a case study of an arid, continental diagenetic facies. Sandstone Diagenesis: Recent and Ancient, pp. 303–320.
Steel, R.J., Thompson, D.B., 1983. Structures and textures in Triassic braided stream conglomerates ('Bunter' pebble beds) in the Sherwood Sandstone group, North Staffordshire, England. Sedimentology 30 (3), 341–367.
Szurlies, M., 2004. Magnetostratigraphy: the key to a global correlation of the classic Germanic Trias-case study Volpriehausen Formation (Middle Buntsandstein), Central Germany. Earth Planet Sci. Lett. 227 (3–4), 395–410.
Toonen, W.H., Kleinhans, M.G., Cohen, K.M., 2012. Sedimentary architecture of abandoned channel fills. Earth Surf. Process. Landf. 37 (4), 459–472.
Tooth, S., 2005. Splay formation along the lower reaches of ephemeral rivers on the Northern Plains of arid central Australia. J. Sediment. Res. 75 (4), 636–649.
Van Adrichem Boogaert, H.A., Kouwe, W.F.P., 1993. Stratigraphic nomenclature of the Netherlands, revision and update by RGD and NOGEPA, section A. Mededelingen Rijks Geologische Dienst. Netherlands 1–40.
Van der Zwan, C.J., Spaak, P., 1992. Lower to Middle Triassic sequence stratigraphy and climatology of the Netherlands, a model. Palaeogeogr. Palaeoclimatol. Palaeoecol. 91 (3–4), 277–290.
Verweij, J.M., 1993. Hydrocarbon Migration Systems Analysis, 35. Elsevier.
Voigt, T., 2017. Die Ablagerungssysteme des Unteren und Mittleren Buntsandsteins in Thüringen. Geowiss. Mittl. Thuringen 14, 39–95.
Walker, T.R., 1979. Red color in dune sands. In: McKee, E.D. (Ed.), A Study of Global Sand Seas. U.S. Government Printing Office, Washington, D. C., pp. 61–81
Weber, K.J., 1982. Influence of common sedimentary structures on fluid flow in reservoir models. J. Petrol. Technol. 34 (3), 665–672.
Yagishita, K., 1997. Paleocurrent and fabric analyses of fluvial conglomerates of the Paleogene Noda group, northeast Japan. Sediment. Geol. 109 (1–2), 53–71.
Zhang, G., Buatois, L.A., Mángano, M.G., Aceñolaza, F.G., 1998. Sedimentary facies and environmental ichnology of a? Permian playa-lake complex in western Argentina. Palaeogeogr. Palaeoclimatol. Palaeoecol. 138 (1–4), 221–243.
Ziegler, P.A., 1982. Geological Atlas of central and Western Europe. Shell International Petroleum Maatschappij. BV, Amsterdam, p. 130.
Ziegler, P.A., Schumacher, M.E., Dèzes, P., Van Wees, J.D., Cloetingh, S.A.P.L., 2004. Post-Variscan evolution of the lithosphere in the Rhine Graben area: constraints from subsidence modelling. Geol. Soc., London, Spec. Publ. 223 (1), 289–317.
Zijerveld, L., Stephenson, R., Cloetingh, S.A.P.L., Duin, E., Van den Berg, M.W., 1992. Subsidence analysis and modelling of the roer valley graben (SE Netherlands). Tectonophysics 208 (1–3), 159–171.